JGR Oceans

RESEARCH ARTICLE
10.1029/2025JC023249

Anomalously Low New Production in the Northeast Atlantic During Spring 2024: A Consequence of Weaker Winter Mixing?

S. C. Painter[1], E. E. García-Martín[1], C. Feltham[1], R. Muliawan[1], E. Mawji[1], K. Peel[1], S. Kelly[1], A. Flohr[1], S. Hartman[1], and A. R. Gates[1]

[1]National Oceanography Centre, Southampton, UK

Key Points:

- A large body of low chlorophyll waters formed and persisted in the NE Atlantic during 2024
- Mean productivity rates and particulate concentrations were 44%–79% lower than surrounding waters
- North Atlantic thermal history was likely a key driver behind weak productivity

Supporting Information:

Supporting Information may be found in the online version of this article.

Correspondence to:

S. C. Painter,
stuart.painter@noc.ac.uk

Citation:

Painter, S. C., García-Martín, E. E., Feltham, C., Muliawan, R., Mawji, E., Peel, K., et al. (2026). Anomalously low new production in the Northeast Atlantic during spring 2024: A consequence of weaker winter mixing? *Journal of Geophysical Research: Oceans*, *131*, e2025JC023249. https://doi.org/10.1029/2025JC023249

Received 1 AUG 2025
Accepted 20 JAN 2026

Author Contributions:

Conceptualization: S. C. Painter
Data curation: S. C. Painter
Formal analysis: S. C. Painter, E. E. García-Martín, E. Mawji, K. Peel, S. Kelly
Funding acquisition: S. Hartman, A. R. Gates
Investigation: S. C. Painter, E. E. García-Martín, C. Feltham, R. Muliawan
Project administration: A. R. Gates
Visualization: S. C. Painter
Writing – original draft: S. C. Painter
Writing – review & editing: S. C. Painter, E. E. García-Martín, C. Feltham, R. Muliawan, E. Mawji, K. Peel, S. Kelly, A. Flohr, S. Hartman, A. R. Gates

Abstract In 2024 an anomalous region of low chlorophyll water covering ~721,000 km^2 or 1.7% of North Atlantic surface area dominated the Northeast Atlantic. This feature formed during spring, remained identifiable as a region of low chlorophyll throughout the summer months in temperate and subpolar waters and, due to low opal ballasting potential of newly formed biomass, likely impacted ecosystem processes and carbon export fluxes across a wide sector of the Northeast Atlantic. In situ sampling along the southern edge of this region for 15 days in May–June encountered an unusually deep euphotic layer that shoaled rapidly from >80 to ~40 m over subsequent days and low surface chlorophyll concentrations (<0.3 mg m^{-3}) despite non-limiting nitrate and phosphate availability, though silicate was exhausted. Integrated net primary production rates within this feature ranged between 0.5 and 0.6 g C m^{-2} d^{-1}, NO_3^- uptake rates between 0.8 and 1.3 mmol N m^{-2} d^{-1}, and new production rates between 0.08 and 0.13 g C m^{-2} d^{-1}; rates that on average were 45%–79% lower than rates outside of this feature. Integrated concentrations of particulate organic carbon (POC), nitrogen (PON) and phosphorous (POP) were up to 44%–63% lower than surrounding waters. We hypothesize that this region of low productivity may be the consequence of prolonged and anomalous warming of the wider North Atlantic throughout 2023–2024 leading to weaker mixing and preconditioning of the surface ocean during winter 2024 with implications for the resident phytoplankton community.

Plain Language Summary This study describes primary production observations collected during the 2024 Northeast Atlantic spring bloom, a period usually associated with high rates of productivity. Instead, spring 2024 was characterized with a large and highly anomalous region of low productivity water that occupied a substantial area of the Northeast Atlantic. Primary production and nitrate uptake rate measurements within this region were on average 45%–79% lower than the surrounding waters. Such significant decreases in productivity during a critical time of year, coupled with low sinking potential of newly produced organic carbon, indicate likely consequences for carbon export to the ocean interior and for energy transference to higher trophic levels. Subsequent investigation links this feature to shallow and later than usual winter convective mixing. The study suggests that increased occurrence of warmer than average winters is likely to increasingly disrupt the timing and intensity of the North Atlantic spring bloom.

1. Introduction

The North Atlantic spring bloom is one of the best studied annually occurring productivity events in the ocean yet it continues to demand attention due to perceived changes in the timing (phenology) (Asch, 2019; Friedland et al., 2016, 2024), and magnitude (Martinez et al., 2011), of the bloom in response to both natural climate variability and anthropogenic climate change (Follows & Dutkiewicz, 2002; Kelly et al., 2025; Sundby et al., 2016). For the temperate Northeast Atlantic the spring bloom typically begins in March/April, peaks in May/June, with maximum primary production rates of 1–1.5 g C m^{-1} d^{-1} and total annual productivity is typically <250 g C m^{-2} (Longhurst, 1995, 1998; Tilstone et al., 2023). The regular and predictable production of photosynthetic biomass during the spring bloom is important for higher trophic levels (e.g., zooplankton, fish) and for carbon sequestration to the ocean interior with around half of the total annual carbon export flux for the North Atlantic region (0.55–1.94 Gt C yr^{-1}) derived from the spring bloom (Sanders et al., 2014). Warmer winter and spring temperatures however lead to lower peak biomass, smaller mean cell size, a shift toward smaller phytoplankton size classes and less efficient energy transference to higher trophic levels (Morán et al., 2010; Sommer & Lengfellner, 2008).

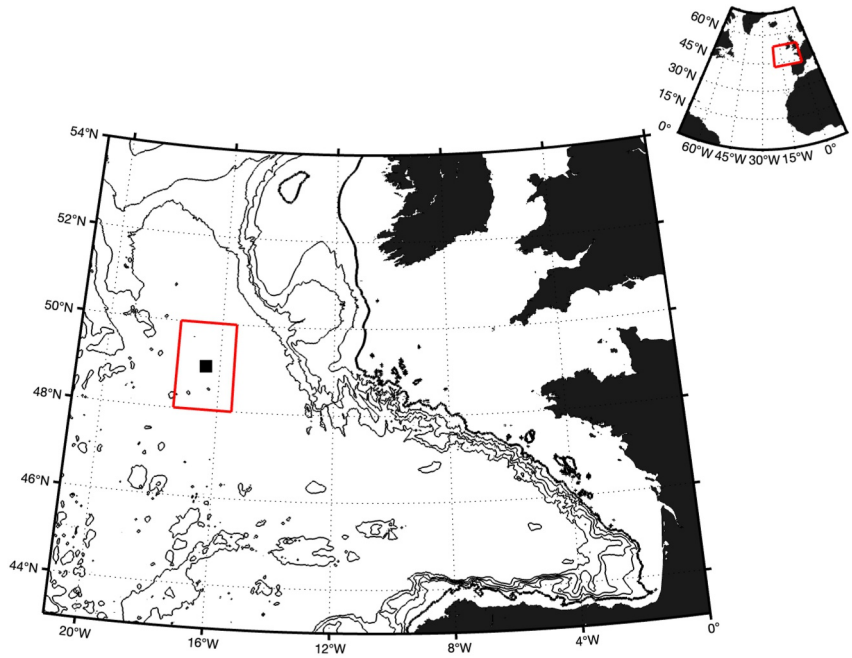

Figure 1. Map showing nominal location of sampling site (black square) relative to the United Kingdom. The red box in the larger image represents the area (2° × 2° longitude/latitude) that remote sensing data shown in Figure 3 were averaged over. The inset map shows the region of the larger image (red box) in context with the wider North Atlantic.

During the 2024 annual cruise in support of the Porcupine Abyssal Plain Sustained Observatory (PAP-SO) program (49°N, 16.5°W; Hartman et al., 2021), an unusual and extensive body of water with low surface chlorophyll was encountered. Sampled during the peak timeframe for the spring bloom this provided an opportunity to explore the notion that aspects of the North Atlantic spring bloom are changing via the study of net primary production (NPP), new production and biomass concentrations. Here we explore the possibility that weak mixing during winter 2024, linked to anomalous warming of the North Atlantic throughout 2023–2024 (Berthou et al., 2024; Carton et al., 2025; Terhaar et al., 2025), was a key factor impacting the productivity of the spring bloom, with consequential impacts for carbon export fluxes and trophic level transference.

2. Methods

2.1. General Setting

Observations were collected in the Northeast Atlantic between 20 May and 12 June 2024 aboard RRS *James Cook* (cruise JC263) (Gates, 2023). All samples were collected within a 1 km radius around a nominal position of 48.98°N 16.368°W (approx. 800 km southwest of Lands End, UK; Figure 1). Sampling dates place this cruise immediately before the mean late June timing of the annual spring bloom at the PAP-SO study site (Painter et al., 2016). Day-to-day variation in sampling position was influenced by the projected position and subsequent exclusion circle of a surface buoy on a deep-water instrumented mooring (water depth ∼4,800 m) (Hartman et al., 2012, 2015). In the following, we report daily pre-dawn profiles of upper ocean primary productivity covering a 15-day period, noting that the last station was sampled after a 2-day gap in sampling due to mooring and other scientific activities.

2.2. Sampling

Water samples for all parameters were collected across the euphotic zone from depths corresponding to irradiance horizons of 97%, 55%, 33%, 14%, 4.5% and 1% of surface PAR (photosynthetically active radiation) using a Seabird 9/11+ CTD and niskin bottle rosette. Sampling depths were adjusted daily based on temporal changes to the attenuation coefficient which was estimated from a regression of natural log normalized irradiance intensity (PAR) against depth. Separate PAR profiles were collected within ±3 hr of local noon and used to inform the

following days sampling depths. Seawater was collected directly from the niskin bottles into acid cleaned 10 L carboys, which were covered with dark screens whilst being processed.

2.3. Nutrients

Seawater samples for nutrient analysis were collected directly from the niskin bottles into acid cleaned 100 ml Nalgene bottles or sterile 50 ml centrifuge tubes and frozen (−20°C) immediately (Becker et al., 2020; Chapman & Mostert, 1990; Dore et al., 1996). Subsequent analysis of samples for nitrate, nitrite, phosphate and silicate used a Seal Analytical (QuAAtro 39) segmented flow-analyzer with XY autosampler and Seal methods; Silicate Q-066-05 Rev. 5, Phosphate Q-064-05 Rev. 8, Nitrate and nitrite Q-068-05 Rev.11, Nitrite Q-070-05 Rev. 6. On the day of analysis water samples were defrosted using a water bath (50°C) for a period of 40 min and allowed to return to room temperature, minimizing loss of reactive silicate (Becker et al., 2020). Analytical detection limits were 0.08 μmol NO_3^- L^{-1}, 0.08 μmol Si L^{-1}, 0.01 μmol NO_2^- L^{-1}, and 0.01 μmol PO_4^{3-} L^{-1}. Certified reference standards lot CL, CI and CS (Kanso Technos Co., Ltd, Japan) were used throughout each analytical run to track accuracy and precision.

2.4. Total Chlorophyll-*a*

Total chlorophyll-*a* concentrations (Tchla) were obtained from 250 ml seawater samples carefully measured from each carboy and filtered onto a 25 mm GF/F grade glass fiber filter. After filtration each filter was immediately placed into a 25 ml glass vial and immersed in 6 ml of 90% acetone to allow pigment extraction. Samples were stored in the dark at 4°C for 18–20 hr before the extracted pigment fluorescence was measured on a Turner Trilogy bench top fluorometer calibrated with a chlorophyll-*a* (Chl-*a*) standard (Sigma-Aldrich, UK).

2.5. Particulate Pools (POC, PON, POP, BSi, PIC)

Particulate organic carbon and nitrogen (POC, PON) concentrations were obtained from 2 L seawater samples filtered onto pre-combusted (450°C for ∼6 hr) glass fiber filters (Whatman GF/F). Filters were rinsed with a 0.25 N solution of HCl (Kennedy et al., 2005) to remove particulate inorganic carbon, placed inside petri-slides, oven dried onboard at 40°C overnight and thereafter stored in sealed petri-slides at ambient room temperature in the dark. Filters were subsequently pelleted into tin capsules and analyzed for carbon and nitrogen elemental and isotopic content using an Elementar Vario elemental analyzer coupled to an Isoprime 100 mass spectrometer (University of Southampton Stable Isotope Ratio Mass Spectrometry laboratory). Final elemental concentrations are reported in units of μmol L^{-1} with natural abundance isotopic content reported in the permil notation relative to the bulk atmospheric air standard for nitrogen (Coplen et al., 1992), or Vienna Peedee belemnite (VPDB) for carbon (Coplen, 1994).

Particulate organic phosphorous (POP) concentrations were measured from 2 L seawater samples filtered onto pre-combusted and acid-cleaned glass fiber filters (Fisher MF300 filters). Before use, filters underwent repeated bathing in 10% HCl and ultrapure water solutions to remove contaminants. After filtration filters were placed into pre-combusted glass test tubes (450°C, >8 hr), oven dried overnight at 40°C before the test tubes were sealed with parafilm. Samples were stored at room temperature until analysis. In the laboratory the phosphorous content of each sample was measured using the digestion method of Karl et al. (1991), with the released phosphorous measured as per standard seawater nutrient methods.

Concentrations of biogenic silica (BSi) were obtained from 0.5 L seawater samples filtered on 25 mm diameter 0.8 μm pore size nucleopore polycarbonate filters. Filters were rinsed with 0.2 μm filtered seawater, placed in plastic test tubes, oven dried overnight at 40°C before being sealed with a screw cap. In the laboratory the captured particulate material was digested via addition of 0.2 M NaOH (Ragueneau & Treguer, 1994) with released Si measured via autoanalyzer as per seawater samples.

Particulate Inorganic Carbon (PIC) concentrations were obtained from 0.5 L seawater samples filtered on to 25 mm 0.8 μm pore size nucleopore membrane filters. Filters were rinsed with borax buffered Milli-Q water, placed in plastic test tubes, oven dried onboard at 40°C overnight and then sealed with a screwcap. In the laboratory the particulate material was digested over 24 hr via the addition of 5 ml of 0.3 M nitric acid. The acid was subsequently syringe filtered through a 0.45 μm PTFE filter and the dissolved calcium content analyzed via ICP-

OES (Green et al., 2003; Poulton et al., 2006). Final PIC concentrations were obtained from the measured calcium content assuming a 1:1 molar equivalence within calcite ($CaCO_3$) (Mitchell & Godrijan, 2025).

2.6. Primary Production

Primary production was measured using the ^{13}C method (Hama et al., 1983; IOCCG et al., 2022). At each depth 2 L seawater samples were carefully measured into duplicate Nalgene polycarbonate bottles, one wrapped with optical filters (Lee Filters, neutral density and misty blue) to replicate in situ irradiance depths (light bottles) and the second with black tape to eliminate all light (dark bottles). Each individual bottle was inoculated with 210 µl L^{-1} of a 0.500 mol L^{-1} stock solution of ^{13}C labeled sodium bicarbonate (Cambridge Isotope Laboratories, >99%) to a final concentration of 105 µmol L^{-1}, or approximately 5% of ambient dissolved inorganic carbon (DIC) concentrations (cruise measured mean surface DIC concentration 2127.5 ± 5.4 µmol kg^{-1}). Bottles were placed into a Fytoscope growth chamber (Photo System Instruments, Czech Republic) to control both ambient light and temperature. The incubator temperature was maintained at 13°C representative of the mixed layer temperature (mean mixed layer temperature 13.3 ± 0.6°C; range 12.7–14.2°C). At this latitude and time of year the daylength was ∼16 hr. Irradiance levels were therefore set to follow a sinusoidal pattern with a light:dark routine of 16:8 hr with a maximum irradiance of ∼1,200 µmols photons m^{-2} s^{-1}. After incubation, samples were filtered onto pre-ashed (450°C for >4 hr) 25 mm glass fiber filters (Whatman GF/F grade) and rinsed with 0.25 N HCl to remove particulate inorganic carbon (Kennedy et al., 2005) before being washed with 0.2 µm filtered seawater and oven dried overnight at 40°C. Samples were subsequently pelleted into tin capsules and analyzed via mass and isotopic content using an Elementar Vario elemental analyzer coupled to an Isoprime 100 mass spectrometer (University of Southampton). Production rates were calculated following Hama et al. (1983) and included a correction (subtraction) for any dark carbon uptake (IOCCG et al., 2022) which on average represented 0.9 ± 0.2% of the light uptake rate for individual bottles. Integrated daily production rates were obtained via trapezoidal integration. Final rates are presumed to represent net primary production.

Community growth rates (µ; d^{-1}) were estimated at all sampled depths following Marañón (2005) and are presented as depth averaged rates per station to evaluate the temporal change in community growth. Growth rates were calculated as

$$\mu = \frac{P^B}{C : \text{Chl } a}$$

where P^B is the chlorophyll normalized carbon production rate (mg C [mg Chl-a]$^{-1}$ d^{-1}) and C: Chl a is the carbon to Chl-a ratio (mg C [mg Chl-a]$^{-1}$).

2.7. Nitrate Uptake and New Production

Nitrate uptake rates were estimated via addition of a ^{15}N-labeled NO_3^- isotopic tracer to each individual primary production bottle (Slawyk et al., 1977). Each bottle (light and dark) was inoculated with 50 µl L^{-1} of a 2 mmol L^{-1} stock solution of ^{15}N labeled sodium nitrate (Cambridge Isotope Laboratories, >99% purity) to a final concentration of 0.1 µmol L^{-1}. In situ nutrient concentrations were unknown at this point. Post-cruise comparison to the actual nutrient data revealed NO_3^- concentrations of 2.6–8.2 µmol NO_3^- L^{-1}, hence the ^{15}N tracer additions which ranged from 1.2% to 3.9% of in situ concentrations, and averaged 2 ± 1% of ambient pools, were less than the nominal 10% addition considered necessary to avoid stimulating uptake (Dugdale & Goering, 1967). Nitrogen elemental mass and isotopic enrichment of the collected particulate material were obtained during dual elemental and isotopic analysis as described above for primary production. Uptake rates were calculated using the equations of Dugdale and Goering (1967).

Dark NO_3^- uptake rates averaged 3.4 ± 2.9% of corresponding light uptake rates in the upper euphotic zone. As NO_3^- uptake was therefore predominantly light driven dark uptake rates were subtracted from the corresponding light uptake rate to produce a dark corrected uptake rate for each bottle. Total daily NO_3^- uptake was obtained by scaling the hourly dark corrected uptake rate by the photoperiod (16 hr). Integrated daily uptake rates were obtained via trapezoidal integration.

New production was approximated for each daily profile by scaling the integrated dark corrected NO_3^- uptake rate by the mean particulate C:N ratio of that profile. This was preferred over use of a fixed C:N as the data set

indicated a significant shift in particulate C:N with time (see results). Individual profile C:N values could deviate from the global mean ratio of 6.625 (Redfield et al., 1963) by up to 34% (e.g., 8.94 vs 6.625). A similar temporal shift was also evident in the C:NO_3^- uptake ratio further arguing against use of a fixed ratio. An integrated *f*-ratio estimate was calculated for each station simply as the ratio of integrated new production to integrated primary production.

2.8. Remote Sensing and Float Data

2.8.1. Satellite Observations

To support the cruise-based observations satellite estimates of sea surface temperature (sst4; (Kilpatrick et al., 2015), chlorophyll-*a* (Hu et al., 2019) and particulate inorganic carbon (Balch et al., 2005; Gordon et al., 2001) at 4 km spatial resolution and at 8-day averaging intervals were obtained from the MODIS Aqua platform via the NASA Ocean Color repository (https://oceancolor.gsfc.nasa.gov). A 20-year mean time series for the period 2002–2022 was produced for a region covering ±1° around the PAP-SO position (i.e., 48–50°N, 15.5–17.5°W; red box in Figure 1) to compare to the 2024 time series averaged over the same geographic region. The year 2023 was excluded from the long-term mean due to documented impacts of a marine heatwave in the Northeast Atlantic in that year (Carton et al., 2025; England et al., 2025; Guinaldo & Neukermans, 2025; Jacobs et al., 2024).

Alternative SST products, the Optimally Interpolated Sea Surface Temperature (OISST; v2.1; (Huang et al., 2021)) and the Operational Sea Surface Temperature and Sea Ice Analysis (OSTIA; (Good et al., 2020)) were also examined due to concerns over temperature artifacts in the Aqua record (see results). Differences between these sea surface temperature data sets are described in Gao et al. (2023).

To interpret surface water and float trajectories relative to regions impacted by marine heat waves preceding the 2024 spring bloom marine heatwave maps for the region 40–60°N 0–36°W for 20 June 2023 were acquired from the Coral Reef Watch repository (https://www.star.nesdis.noaa.gov/pub/socd/mecb/crw/data/marine_heatwave/v1.0.1/category/). Marine heatwave classification followed Hobday et al. (2016, 2018).

2.8.2. Float Observations

Surface drifter float trajectories at 6-hourly resolution for the region 45–55°N, 5–25°W and for the time period 1 June 2023 to 1 June 2024 were obtained from the Global Drifter program (Lumpkin & Centurioni, 2019). Data were accessed via the NOAA ERDAP server (https://www.aoml.noaa.gov/phod/gdp/interpolated/data/all.php). These data were examined to allow tracking of surface water advective pathways over the preceding 12 months prior to sampling.

Profiling float data were obtained from the global Argo array (Argo, 2000) for a region ±3° around our study site (46–52°N, 13.5–19.5°W) and covering 1st Jan to 1st May for each year from 2020 to 2024. These data were used to examine both the subsurface thermal history of waters around the study site during the winter and early spring period immediately before sampling and to contrast upper ocean conditions in 2024 with those of recent years. Mixed layer depths were calculated using a density threshold criteria of +0.03 kg m^{-3} relative to 10 m (de Boyer Montegut et al., 2004).

2.9. Statistical Analyses and Data Handling

Pearson's correlation was used to determine relationships between key biological and environmental variables with a significance criterion of 0.05. All statistical analyses were performed in *R* version 4.4.2 (R Core Team, 2024).

In the following a distinction is drawn between results for stations 1 to 6 and results from stations 7 to 13. These two groups of stations can be distinguished due to the passage of a hydrographic/biological front through the study site between days 6 and 7 (Figure S1 in Supporting Information S1). This places stations 1 to 6 within the low chlorophyll anomaly, and stations 7 to 13 outside of this feature.

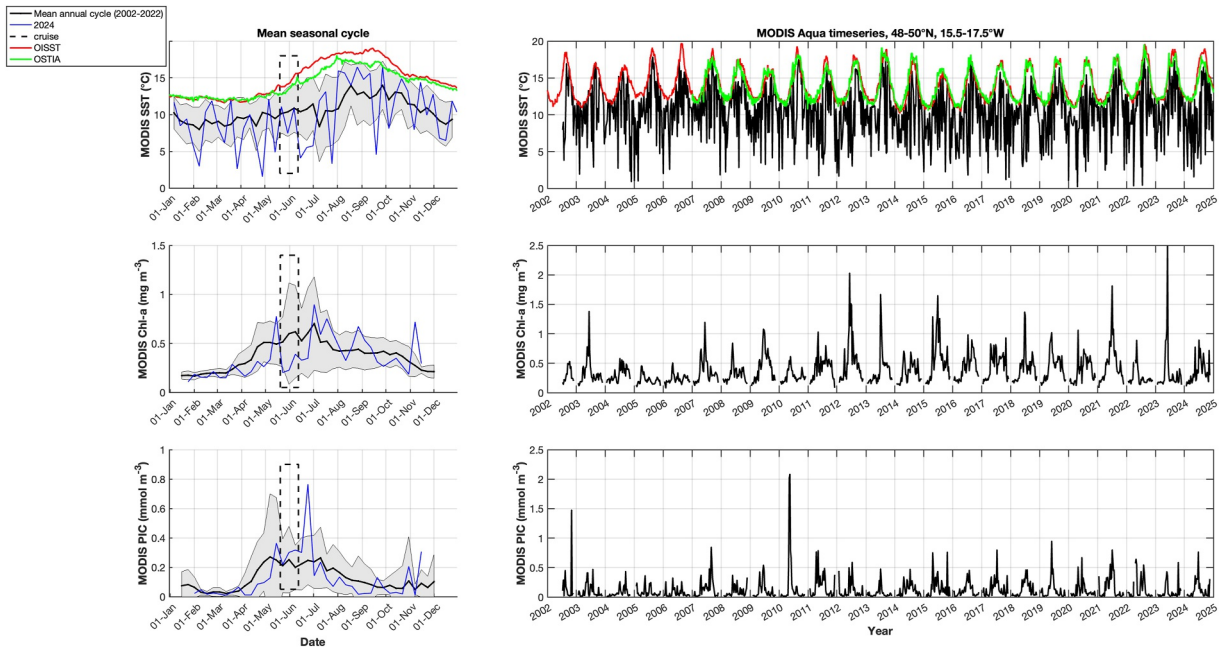

Figure 2. Modis Aqua timeseries of upper ocean variability showing in the left column the mean annual cycles of sea surface temperature (SST4), chlorophyll (Chl-a) and particulate inorganic carbon (PIC) for the period 2002–2023 (black line with shading to illustrate the standard deviation) in relation to the time series for 2024 (blue line). Panels on the right present the 2002–2024 time series of sea surface temperature, chlorophyll and particulate inorganic carbon. Both the mean annual cycles and the timeseries cover a 2° by 2° region of the northeast Atlantic centered upon the nominal location of the PAP-SO (49°N, 16.5°W). Black dashed box indicates dates of in situ sampling.

3. Results

3.1. Seasonal Context From Remote Sensing

Satellite observations of sea surface temperature showed strong fluctuations with temperatures that at times were 1–3°C below the 2002–2022 average (Figure 2). Satellite chlorophyll concentrations both during and immediately after the in situ sampling period were lower than average (~0.2–0.4 μg L^{-1} vs ~0.6 μg L^{-1}), whilst PIC concentrations of ~0.3 mmol m^{-3} were above the 2002–2022 average of ~0.2 mmol m^{-3} but within historic ranges. Unusually, there was no obvious peak in chlorophyll to signify the spring bloom. A large peak in PIC concentrations was evident in late June but this occurred after sampling had finished. Spring 2024 was therefore marked by highly variable SST, below average chlorophyll and above average PIC concentrations (Figure 2).

Extensive cloud cover during the cruise period necessitated spatial averaging over a comparatively large area (~2° × 2°) to obtain the seasonal trends shown in Figure 2. As infrared radiometers are susceptible to clouds, water vapor, air pollution, and aerosols (Gao et al., 2023; Guan & Kawamura, 2003; Kilpatrick et al., 2015) the combination of extensive cloud cover and large-scale averaging may explain the erratic behavior of the SST record, though this impact is not as obvious in the chlorophyll or PIC records. Alternative OISST and OSTIA SST products for 2024 are also included in Figure 2 which reinforce the presumption that the large swings in MODIS SST are artifacts rather than real phenomena.

3.1.1. Wider North Atlantic

The weak appearance of the spring bloom in the satellite chlorophyll record shown in Figure 2 prompted further analysis of monthly averaged surface chlorophyll composite images for the wider North Atlantic region which indicated the formation and persistence of an anomalous body of water with low chlorophyll concentrations (<0.25 mg m^{-3}) across the eastern North Atlantic between spring and autumn 2024 (Figure 3). This feature was first evident in May, appearing as two almost distinct regions stretching across temperate and subpolar latitudes (~48–62°N), before deepening and repositioning to waters west of Ireland. Minimum chlorophyll concentrations within the central core of this feature were <0.15 mg m^{-3}, thus comparable to waters further south at 35°N. A region of low chlorophyll persisted in the Northeast Atlantic for almost 6 months from spring into early autumn

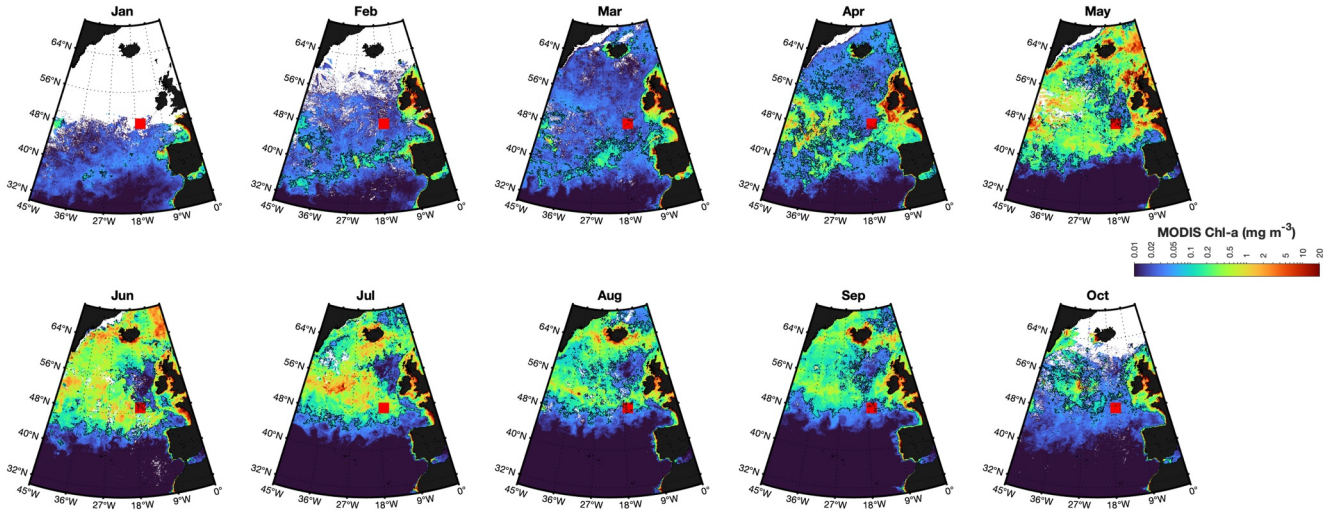

Figure 3. Modis Aqua monthly averages of surface chlorophyll concentration in the North Atlantic during 2024. Note that the images have been scaled to accentuate the regional anomaly evident between May and September.

and only disappeared when chlorophyll concentrations in surrounding waters reduced removing the spatial contrast. In June, coincident with the cruise observations reported here, these low chlorophyll waters occupied an area of ~721,000 km^2, or roughly 1.7% of the North Atlantic surface area (assumed to be 41,490,000 km^2). By August the spatial extent of these waters had reduced by ~15%–~618,000 km^2. The monthly composites suggest a minor northward movement of the center of this feature over the summer from ~50°N in May to 57°N in September. This feature was over twice the size of the combined surface area of Ireland and Great Britain. In situ sampling occurred along the southern border of this feature (Figure 3; Figure S1 in Supporting Information S1).

Further investigation of surface chlorophyll and temperature anomalies for 2024 are shown in Figures S2 and S3 of Supporting Information S1 respectively. Chlorophyll concentrations were lower than the 1997–2023 monthly climatological mean for the months of March to May at the PAP-SO study site. Within the central waters of the chlorophyll anomaly, which moved progressively northwards throughout 2024, concentrations were below monthly climatological conditions until October. Chlorophyll concentrations were most strongly below average throughout June to August with reductions relative to the climatological mean approaching 90%. Temperature anomalies indicate sea surface temperatures at the PAP-SO study site were up to 1° warmer than the 1991–2023 climatological mean between January and March, but close to long-term average conditions during April to August. No obvious temperature anomaly could be associated with the region of low chlorophyll.

3.2. In Situ Environmental Conditions

3.2.1. Hydrography

Upper ocean hydrographic conditions changed from cooler and fresher waters (~12.7°C; ~35.76 g kg^{-1}) to warmer and more saline surface waters (~14.2°C; 35.91 g kg^{-1}) over the observation period (Figure 4). These changes were coincident with increases in chlorophyll fluorescence from ~0.2 to ~2 µg L^{-1}, dissolved oxygen concentrations from 260 to 270 µmol L^{-1} and turbidity leading to a decline in the optical clarity of the water column, an increase in light attenuation from unusually low values of 0.055 m^{-1} at the start of sampling to more typical values of 0.1098 m^{-1} by the end of sampling and a shoaling of the euphotic zone from 84 to 42 m. Environmental conditions in the surface mixed layer were stable and comparable during days 1–6 before changing abruptly from day 7 onwards; a transition attributed to the westward advection of a hydrographic/biological front through the sampling site which placed stations 1 to 6 within the low chlorophyll feature and stations 7 to 13 outside of the low chlorophyll feature (Figure S1 in Supporting Information S1). This resulted in several changes to upper ocean hydrographic conditions including an increase in the mean mixed layer conservative temperature from 12.8 ± 0.1°C to 13.8 ± 0.4°C and an increase in salinity (S_A) from 35.76 ± 0.02 to 35.85 ± 0.04 g kg^{-1}.

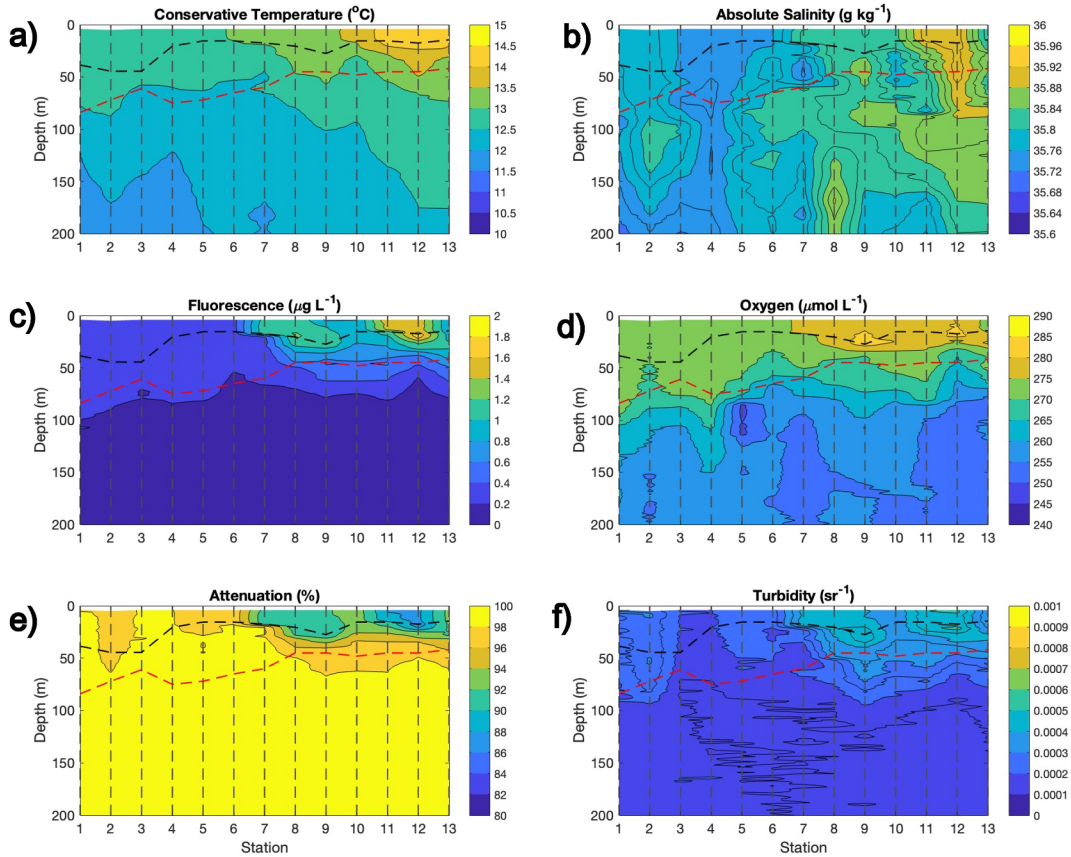

Figure 4. Time series of upper ocean (0–200 m) hydrographic conditions including (a) conservative temperature, (b) absolute salinity, (c) chlorophyll fluorescence, (d) dissolved oxygen concentrations, (e) light attenuation and (f) water column turbidity. Indicated are the surface mixed layer (dashed black line) and euphotic depth (red dashed line).

3.2.2. Nutrients

Surface nutrient concentrations were mesotrophic being above summer minimum concentrations (~0.1 μmol L^{-1}) but below typical winter maximum concentrations for the region. Surface macronutrient concentrations ranged from 2.64 to 6.06 μmol NO_3^- L^{-1}, 0.6–1.71 μmol Si L^{-1}, and 0.18–0.36 μmol PO_4^{3-} L^{-1} (Figure 5).

Mixed layer nutrient concentrations averaged over the observation period were 4.72 ± 1.16 μmol NO_3^- L^{-1}, 1.15 ± 0.43 μmol Si L^{-1} and 0.3 ± 0.07 μmol PO_4^{3-} L^{-1} and comparatively depleted compared to winter conditions (e.g., 8–11 μmol NO_3^- L^{-1} (Boyer et al., 2013; Hartman et al., 2010, 2015; Koeve, 2001). Nutrient concentrations varied temporally in tandem with changes to hydrographic conditions, but also revealed subsurface structure linked to water column stratification and to nutrient recycling (e.g., nitrite). As with the hydrography, nutrient concentrations were similar and comparatively high for the first 6 days before decreasing rapidly from day 7 onwards. This was evident as changes in the mean mixed layer concentrations of NO_3^- and PO_4^{3-} which reduced from 5.74 ± 0.18 to 3.85 ± 0.86 μmol L^{-1} and 0.36 ± 0.03 to 0.25 ± 0.05 μmol L^{-1} respectively (~30% reductions) but mean Si concentrations diverged from this trend and increased from 0.81 ± 0.31 to 1.44 ± 0.28 μmol L^{-1} (~80% increase) due to significant variability in subsurface silicate concentrations (Figure 5). NO_2^- distributions revealed the presence of a patchy subsurface maximum with concentrations >0.3 μmol NO_2^- L^{-1} that shoaled from ~150 to ~75 m and which remained below the base of the euphotic zone suggesting a link to local remineralization processes. NO_2^- concentrations at the maximum were generally twice those measured in surface waters.

Nutrient (N:Si:P) ratios within surface waters indicated balanced availability of N and P with respect to a global mean of 16:1 but severe Si limitation. The cruise average N:Si:P stoichiometric ratio for surface waters was

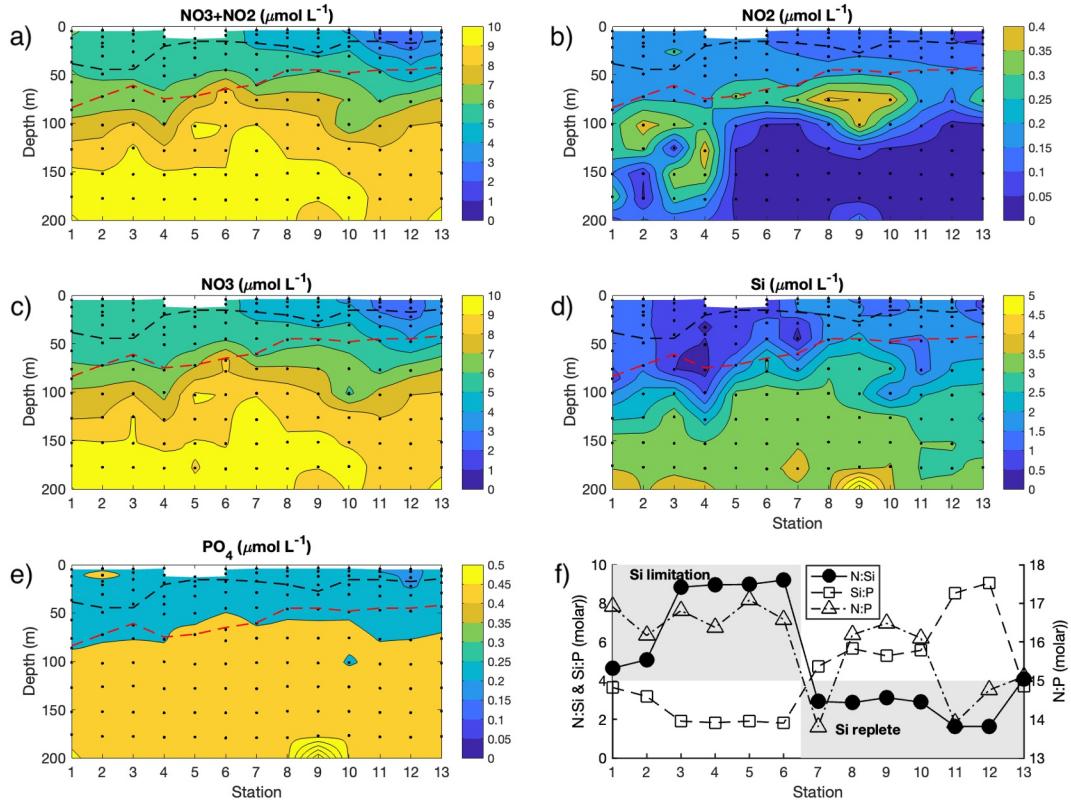

Figure 5. Time series of upper ocean (0–200 m) nutrient concentrations showing (a) total nitrate ($NO_3^- + NO_2^-$), (b) Nitrite (NO_2^-), (c) Nitrate (NO_3^-), (d) Silicate (Si), (e) Phosphate (PO_4^{3-}) and (f) surface nutrient stoichiometries. The surface mixed layer is indicated by the black dashed line and the euphotic depth by the red dashed line in panels (a–e).

15.9:4.4:1, but this mean was not indicative of the temporal variation evident between stations due to changes in Si concentrations. Stations 1 to 6 therefore had a mean of 16.7:2.4:1 whereas stations 7 to 13 averaged 15.2:6.1:1.

N:P molar ratios were broadly comparable between all stations ranging from 13.8:1 to 17.1:1, and averaging 15.9 ± 1.1. No discernible temporal trend in N:P was evident. Ratios of N:Si however, were far more variable ranging from 1.6:1 to 9.2:1 (mean 5.0 ± 2.9) with high ratios a characteristic of the earlier stations (Figure 5). Surface N:Si values at station 1 to 6 consistently exceeded 4:1 reaching as high as 9.2:1 at station 6, whereas for stations 7–13 N:Si values were lower and typically <3:1. Ambient N:Si ratios >4 have been shown to induce Si limitation within diatoms (Gilpin et al., 2004), thus the nutrient data implied severe Si stress at stations 1 to 6 and a transition from high Si stress to low Si stress conditions during the cruise.

3.2.3. Light Field

Maximum incident PAR measured by ship bridge top PAR sensors was typically in the range of 200–500 W m^{-2} s^{-1} (Figure S4 in Supporting Information S1). The duration of the daily irradiance cycle was well recreated by the Fytoscope growth chamber but peak incident PAR around solar noon could exceed the maximum irradiance levels produced by the growth chamber. Allowing for the imprecision in converting from scalar to quantum units maximum daily PAR ranged from 1,350 to 2927 μmol photons m^{-2} s^{-1}. Daily integrated PAR ranged from 20.4 to 58.3 mols photons m^{-2} d^{-1} and was comparable to 8-day averaged estimates of PAR obtained from the MODIS Aqua platform.

3.3. Particulate Data

POC concentrations ranged from 3.2 to 16.5 μmol C L^{-1}, PON from 0.2 to 2.5 μmol N L^{-1}, POP from 0.02 to 0.18 μmol P L^{-1}, BSi from 0.02 to 3.1 μmol Si L^{-1} and PIC from 0.7 to 9.4 μmol C L^{-1}. Concentrations of all pools generally increased with time though not necessarily in step with one another or to the same extent

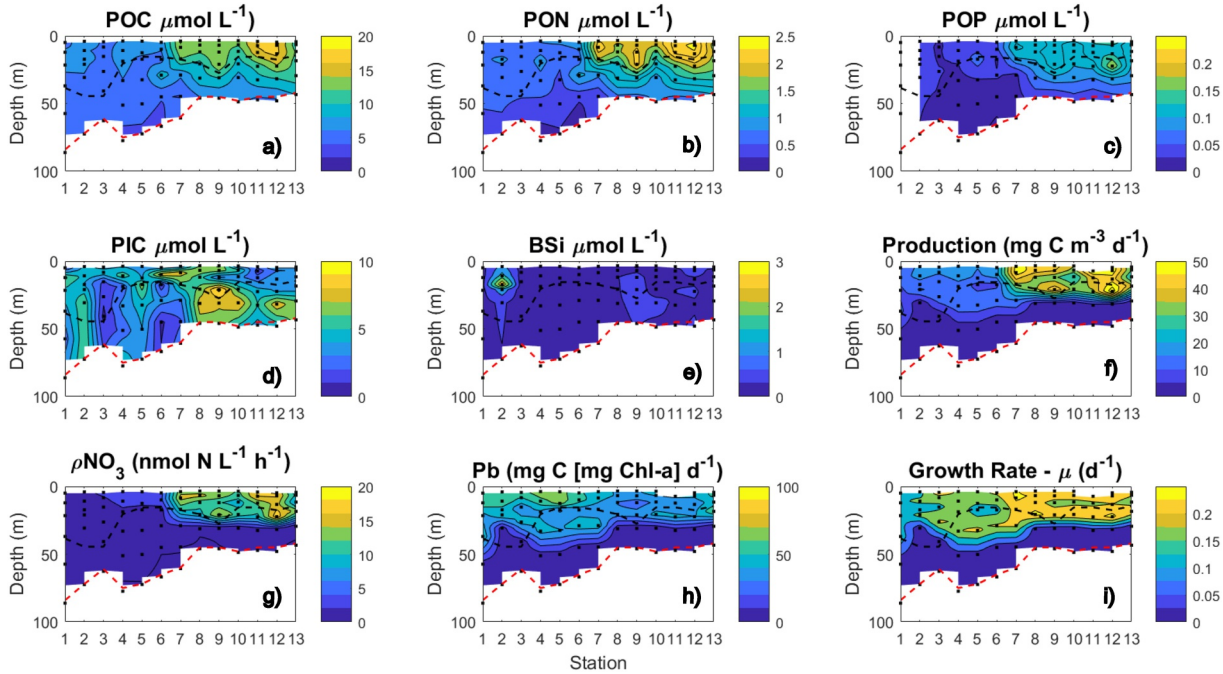

Figure 6. Time series of euphotic zone particulate concentrations and productivity rates including (a) particulate organic carbon (POC), (b) particulate organic nitrogen (PON), (c) particulate organic phosphorous (POP), (d) particulate inorganic carbon (PIC), (e) biogenic silica (BSi), (f) primary production, (g) nitrate uptake (ρNO_3), (h) chlorophyll normalized productivity (Pb) and (i) community growth rates. Indicated are the surface mixed layer (black dashed line) and euphotic depth (red dashed line).

(Figure 6). Specifically, whilst POC, PON and POP broadly followed the same temporal pattern of increasing with time, particularly within the mixed layer, PIC did not follow this pattern exhibiting day-to-day variations that were not replicated within the POC, PON or POP pools. A prominent subsurface maximum in PIC where concentrations reached over 9 μmol C L^{-1} also appeared beneath the mixed layer toward the end of the observation period that was clearly separated from the biomass pools of the mixed layer above. Maximum mixed layer PIC concentrations occurred on day 9, whilst POC, PON and POP peaked on day 12. Mean mixed layer BSi concentrations increased slowly from concentrations <0.4 μmol Si L^{-1} to concentrations of ~0.5 μmol Si L^{-1} but there was no significant increase comparable to that seen in the POC concentrations on day 7 implying that BSi and POC were decoupled.

Concentrations of particulate inorganic carbon were equivalent to 9%–157% (mean ± s.d. 57 ± 31%) of corresponding POC concentrations. POC:PIC ratios (mol:mol) ranged from 0.6 to 11.0 (average ± s.d. of 2.45 ± 1.76).

Euphotic zone integrated POC concentrations ranged from 312 to 553 mmol C m^{-2}, PON from 38 to 78 mmol N m^{-2}, POP from 2.3 to 5.5 mmol P m^{-2}, BSi from 11.8 to 76.6 mmol Si m^{-2} and PIC from 112 to 374 mmol C m^{-2} (Table 1). Integrated concentrations of POC, PON and POP increased with time despite the coincident reduction in the depth of the euphotic zone. To compensate for this behavior depth normalized concentrations of POC, PON and POP were calculated which increased by 224%, 281% and 340% respectively (Figure S5 in Supporting Information S1). Integrated PIC concentrations were more variable and exhibited a decreasing trend with time whilst integrated BSi concentrations remained relatively constant (Table 1). Depth normalized concentrations of PIC and BSi indicated a weak increase with time for PIC and a weak decrease for BSi. Integrated particulate concentrations were up to 44%–63% lower at stations 1 to 6 than at stations 7 to 13.

As a result of the various temporal changes to the particulate concentrations the stoichiometry (C:N:P:Si) of particulate within the euphotic zone also varied (Table 1). This was most clearly evident as a gradual reduction in the C:N molar ratio from ~8.9 to 6.9 with a clear step-change between stations 6 and 7 but equally evident in N:P and C:P ratios which also changed at this point. C:Si ratios increased with time from ~15.5 to 28.7 signifying an increase in POC over BSi. Stoichiometric ratios for the combined particulate pools ranged from 99.3 C : 13.6 N : 1 P : 4.4 Si to 155.4 C : 17.9 N : 1 P : 10.2 Si revealing considerable plasticity (Table 1). The potential for opal to

Table 1
Euphotic Zone Integrated Particulate Concentrations, Integrated Stoichiometry of the Particulate Pool and PIC:POC Ratio

Stn	Date (d/m/y)	Lat (°N)	Lon (°W)	PON (mmol N m^{-2})	POC (mmol C m^{-2})	POP (mmol P m^{-2})	BSiO2 (mmol Si m^{-2})	PIC (mmol C m^{-2})	C:N:P:Si	PIC:POC (molar)
1	26/5/24	48.9750	16.3583	52.2	466.4	–	29.90	308.3	–	0.66
2	27/5/24	48.9752	16.3580	51.2	442.4	3.31	76.57	374.2	133.8:15.5:1:23.2	0.85
3	28/5/24	48.9750	16.3581	37.5	311.9	2.25	14.62	112.2	138.9:16.7:1:6.5	0.36
4	29/5/24	48.9747	16.3583	48.0	409.0	2.69	23.07	262.2	152.2:17.9:1:8.6	0.64
5	30/5/24	48.9747	16.3582	41.5	358.3	3.12	11.79	306.9	115:13.3:1:3.8	0.86
6	31/5/24	48.9752	16.3571	42.1	365.2	2.35	23.94	156.6	155.4:17.9:1:10.2	0.43
7	01/6/24	48.9761	16.3562	66.5	487.3	3.74	16.51	214.5	130.1:17.8:1:4.4	0.44
8	02/6/24	48.9792	16.3615	61.2	441.7	3.93	19.16	295.3	112.3:15.6:1:4.9	0.67
9	03/6/24	48.9870	16.3607	71.9	506.1	4.80	27.41	306.8	105.4:15:1:5.7	0.61
10	04/6/24	48.9840	16.3589	58.4	425.9	4.29	18.87	263.8	99.3:13.6:1:4.4	0.62
11	05/6/24	48.9883	16.3649	71.3	505.8	4.43	20.21	165.5	114.3:16.1:1:4.6	0.33
12	06/6/24	48.9815	16.3651	77.8	552.7	5.48	23.43	225.9	100.9:14.2:1:4.3	0.41
13	09/6/24	48.9799	16.3805	65.4	452.4	3.88	15.77	191.5	116.6:16.9:1:4.1	0.42

ballast POC flux to depth was evaluated via the molar BSi:POC ratio which ranged from <0.01 to 0.45 and averaged 0.06 + 0.06. Most ratios in euphotic zone were <0.1 suggesting weak ballasting potential. Integrated BSi:POC ratios were comparable and low ranging from 0.03 to 0.17.

3.4. Primary Production

Primary production rates within individual bottles ranged from 0.03 to 54.2 μg C L^{-1} d^{-1} and increased over time within the mixed layer (Figure 6). Euphotic zone integrated production rates ranged from 0.5 to 1.27 g C m^{-2} d^{-1} and exhibited a sharp increase between days 6 and 7 commensurate with the environmental changes described above (Table 2). Rates measured during days 1–6 averaged 0.55 ± 0.04 g C m^{-2} d^{-1}, whereas integrated production rates doubled and averaged 1.0 ± 0.18 g C m^{-2} d^{-1} during days 7–13.

Primary production rates integrated across the mixed layer accounted for 68 ± 21% of total primary production integrated across the euphotic layer, implying that around a third of total primary production was occurring in the depth interval between the base of the mixed layer and the base of the euphotic zone. This mixed layer contribution to total column integrated primary production did not change between the pre-front (stations 1–6) and post-front (stations 7–13) stations (68 ± 25% and 68 ± 18% respectively). Deep productivity maxima occurring beneath the mixed layer were evident only toward the end of our sampling period (Figure S6 in Supporting Information S1), but are widely reported for this part of the Northeast Atlantic and generally make a significant contribution to total integrated primary production (Cornec et al., 2021; Hemsley et al., 2015).

Dark carbon fixation rates were measured in parallel but found to be insignificant. Dark carbon fixation accounted for 1.4 ± 0.2% of integrated primary production rates, a result consistent across all mixed layer incubation bottles where dark carbon uptake represented 0.9 ± 0.2% of the corresponding light bottle fixation rates. At the base of the euphotic zone dark carbon uptake as a proportion of the parallel light bottle rate increased reaching between 34% and 84% of the light bottle rate. This increase was driven by the strong decrease in light driven rates with depth and not by a change in the dark fixation rate itself which remained constant with depth (Figure S6 in Supporting Information S1).

Depth averaged community growth rates ranged from 0.09 to 0.16 d^{-1} (Table 2) with maximum growth rates per station ranging from 0.15 to 0.27 d^{-1}. Mean growth rates for stations 1–6 and stations 7–13 exhibited a small but significant increase from 0.11 ± 0.02 d^{-1} to 0.15 ± 0.02 d^{-1} (*t*-test, $p < 0.05$).

Table 2
Euphotic Zone Integrated Rates of Total Chlorophyll, Primary Production, NO_3^- Uptake, New Production, f-Ratio and the Depth Averaged Community Growth Rate

Stn	Total Chl-*a* (mg m^{-2})	Primary production (g C m^{-2} d^{-1})	ρNO3 (mmol N m^{-2} d^{-1})	New production (g C m^{-2} d^{-1})	*f*-ratio	Growth rate (d^{-1})
1	19.7	0.54	0.77	0.08	0.15	0.09
2	21.6	0.57	0.94	0.10	0.17	0.10
3	18.8	0.54	1.01	0.10	0.19	0.13
4	21.0	0.62	1.26	0.13	0.21	0.13
5	20.8	0.53	1.21	0.12	0.24	0.12
6	15.7	0.51	1.14	0.12	0.23	0.12
7	33.6	1.13	4.85	0.43	0.38	0.16
8	43.0	0.96	4.50	0.39	0.41	0.16
9	46.8	1.02	5.23	0.44	0.43	0.15
10	36.9	0.81	4.31	0.38	0.47	0.15
11	38.3	1.06	5.04	0.43	0.40	0.11
12	47.8	1.27	6.62	0.56	0.44	0.16
13	29.1	0.76	3.86	0.32	0.42	0.14

3.5. Nitrate Uptake and New Production

Nitrate uptake rates ranged from ~0 to 17.6 nmol L^{-1} h^{-1}, being highest in near surface waters (<20 m) and decreasing with depth (Figure 6; Figure S7 in Supporting Information S1). Integrated uptake rates ranged from 0.8 to 6.6 mmol NO_3^- m^{-2} d^{-1} but displayed a marked temporal pattern with lower rates at the first 6 stations (mean 1.06 ± 0.18 mmol NO_3^- m^{-2} d^{-1}) before increasing over 4-fold to an average of 4.91 ± 0.88 mmol NO_3^- m^{-2} d^{-1} for the last 7 stations (Table 2).

Rates of new production ranged from 0.08 to 0.56 g C m^{-2} d^{-1} (~6.9–47.0 mmol C m^{-2} d^{-1}) equivalent to an f-ratio of 0.15–0.47 (mean 0.32 ± 0.12) (Table 2) and generally increased with time. This pattern was in line with increased integrated NO_3^- uptake across the euphotic zone and changes to mean mixed layer NO_3^- concentrations which decreased by 46% over the observation period. Rates of new production could be up to 86% higher outside of the low chlorophyll region (station 7 to 13) than within (stations 1 to 6).

Dark NO_3^- uptake was minimal in all incubation bottles with rates ranging from 0.01 to 0.5 nmol N L^{-1} hr^{-1}. Rates were generally invariant with depth (<0.2 nmol N L^{-1} hr^{-1}) though the highest dark uptake rates were often located in the upper 20 m of the water column (the mixed layer). Integrated dark NO_3^- uptake rates ranged from 0.03 to 0.1 mmol NO_3^- m^{-2} d^{-1} and appeared to increase slightly with time a feature attributed to changes in overall water column productivity and perhaps to changes in the phytoplankton community.

3.6. Chlorophyll Concentrations

Total chlorophyll-a concentrations ranged from 0.09 to 1.35 (cruise mean 0.6 ± 0.38) μg L^{-1} and for the mixed layer averaged 0.23–1.23 μg L^{-1}. Mean mixed layer concentrations of 0.23–0.34 μg L^{-1} at stations 1 to 6 were in good agreement with MODIS chlorophyll estimates (~0.3 g L^{-1}; Figure 2) and consistent with weakly productive waters (Figure 3). From day 7 chlorophyll concentrations increased sharply reaching 1.23 μg L^{-1} and at their highest were over 5-fold higher than concentrations observed at stations 1 to 6. Euphotic zone integrated chlorophyll concentrations ranged from 15.7 to 47.8 mg m^{-2} (Table 2) with the mean concentration of 19.6 ± 2.1 for stations 1–6 being half the mean concentration of 39.4 ± 6.9 mg m^{-2} at stations 7–13.

3.7. Environmental Correlations

Total chlorophyll correlated positively with primary production, nitrate uptake and with concentrations of POC, PON and POP ($r^2 > 0.55$, $p < 0.05$; Figure S8 in Supporting Information S1). Total chlorophyll was negatively correlated with concentrations of NO_3, NO_2 and PO_4^{3-} ($r^2 > 0.46$, $p < 0.05$) but positively correlated with Si ($r^2 = 0.36$, $p < 0.05$). Primary production and nitrate uptake were highly correlated ($r^2 = 0.95$, $p < 0.05$) confirming the autotrophic nature of nitrate uptake. In addition, primary production and nitrate uptake were highly correlated

with POC, PON and POP (production $r^2 > 0.73$, $p < 0.05$; ρNO_3 $r^2 > 0.81$, $p < 0.05$). POC, PON and POP were significantly linearly correlated with one another ($r^2 > 0.90$, $p < 0.05$). BSi and PIC did not correlate with production, nitrate uptake or with the organic particulate pools suggesting a decoupling of the biomineral pools from the major organic particulate pools. This decoupling could indicate the presence of detrital or lithogenic material. Strong negative correlations were identified between POC, PON, POP and ambient nutrients pools. These correlations were POC ($r^2 > 0.66$, $p < 0.05$), PON ($r^2 > 0.69$, $p < 0.05$) and POP ($r^2 > 0.64$, $p < 0.05$). BSi and PIC exhibited no correlation with ambient macronutrient pools. Strong negative correlations existed between production, nitrate uptake and the nutrient pools, with the exception of Si. Excluding Si nutrient concentrations explained >43% of the variance in productivity rates ($r^2 > 0.43$, $p < 0.05$), whereas NO_3^- alone explained 60% of the variance in nitrate uptake ($r^2 = 0.6$, $p < 0.05$). Less than 11% of the variation in either primary production or nitrate uptake could be attributed to variation in ambient Si concentrations. This is interpreted to indicate a lack of silicifying plankton contributing to either primary production or nitrate uptake, a reasonable assumption given the low BSi biomass, low ratio values for BSi:POC, low ambient Si concentrations and high N:Si values.

4. Discussion

4.1. The 2024 Spring Bloom in Context

Annual sampling of the Northeast Atlantic spring bloom within the objectives of the PAP-SO program (Hartman et al., 2021) coincided with the presence of a large low chlorophyll feature identifiable in satellite data. In situ sampling within this feature revealed atypical conditions characterized variously by a deep euphotic layer, moderate to low surface nutrient concentrations and low surface chlorophyll concentrations. Mean rates of primary production and nitrate uptake were 45% and 79% lower respectively within this feature (stations 1 to 6) compared to stations sampled outside of this feature (stations 7 to 13). Integrated particulate pools were also up to 44%–63% lower confirming weak productivity characterized this expansive low chlorophyll feature.

Yet not all measured variables align with the characterization of a weak bloom. Low surface silicate concentrations (<2 μmol L^{-1}) suggest prior removal though there is limited indication from the remote sensing timeseries that surface chlorophyll peaked early or widely to support extensive prior nutrient drawdown (Figures 2 and 3), whilst the monthly chlorophyll anomaly maps do not indicate elevated chlorophyll biomass (Figure S2 in Supporting Information S1). Moreover, the presence of severe Si limitation in surface waters, as indicated by high ambient N:Si ratios may actually have inhibited widespread or early productivity (Gilpin et al., 2004; Figure 5). Previous observations of low silicate and high nitrate concentrations during the spring bloom have been associated with shifts in the phytoplankton community from diatoms toward small flagellates (Sieracki et al., 1993). Particulate concentrations, though variable, were nevertheless comparable to previous observations from this region. For example, Leblanc et al. (2009) reported concentrations of POC < 15 μmol C L^{-1}, PON < 2.5 μmol N L^{-1}, POP < 0.3 μmol P L^{-1}, and BSi < 0.25 μmol Si L^{-1} during the late spring bloom period in 2005, which with the exception of BSi are all comparable to the maximum concentrations reported here. Elsewhere, Leblanc et al. (2005) reported peak BSi concentrations of 0.61–0.88 μmol Si L^{-1} during the peak of the Northeast Atlantic spring bloom, which is still considerably lower than the maximum BSi concentration observed here (>3 μmol Si L^{-1}). Air-mass back trajectory modeling (Text S2 in Supporting Information S1) provides credible grounds to infer lithogenic dust inputs from Greenland early in the observation period which may explain the high BSi measurements, particularly as the BSi method is known to be susceptible to lithogenic silica (Ragueneau & Treguer, 1994; Ragueneau et al., 2005; Figure S9 in Supporting Information S1). Despite this source of contamination, the observed BSi:POC ratios were low implying both weak contribution by silicifying phytoplankton to surface POC pools and limited potential for ballasting of POC fluxes with opal. The maximum PIC concentration was high by global standards (Diaz-Rosas et al., 2025; Mitchell et al., 2017; Mitchell & Godrijan, 2025) but at over 9 μmol C L^{-1} was still lower than concentrations of over 11 μmol C L^{-1} reported from neighboring waters by Daniels et al. (2012) and Leblanc et al. (2009). The apparent mismatch between high in situ PIC concentrations versus low surface PIC concentrations observed by satellite (Figure 2) argues for PIC contributions from non-coccolithophore sources. Limited in situ surface sampling of the coccolithophore community during the cruise indicated low cellular abundances (data not shown).

Table 3
Selected Literature Estimates of Primary Production in the Northeast Atlantic

Sampling date	Location	Integrated production (mmol C m^{-2} d^{-1})	Reference	Notes
Aug 1988	38–46°N, 20°W	16–54	Frazel and Berberian (1990)	Total size fraction
Apr/May 1989	47°N, 20°W	90–130	Chipman et al. (1993)	Total size fraction
May/Jul 1989	47–59°N, 20°W	20–96	Joint et al. (1993)	Sum of fractions
May 1990	48.5–50°N, 17–19°W	38–164	Bury et al. (2001)	Sum of fractions
Jul 1990	37–57°N, 20°W	8–106	Donald et al. (2001)	Total size fraction
Jan–Sep 2001	38–45°N, 16–22°W	35–103	Fernandez et al. (2005)	Mean seasonal observations over annual cycle (winter to summer)
May 2004	49°N, −16.4°W	33	Painter et al. (2007)	Single profile
May/Jun	NADR province	86	Tilstone et al. (2009)	NADR province maximum (multi-year estimate)
Jun/Jul 2006	~49°N, 16.5 W	33–111	Painter et al. (2010)	Eddy influenced
Jun 2013	48.6°N, 16.1°W	96–323	Painter, previously unpublished	Unusually high, but so was surface chlorophyll in 2013
May to Jul 1989/1990	46–48.5°N, 15–20°W	19–157	Mattei and Scardi (2021)	Database—various sources but all May to July in 1989 or 1990
May 2021	48.7–49.3°N, 15°W	25–119	Meyer et al. (2024)	Total size fraction
Jul	NE Atlantic including part of NADR	95	Tilstone et al. (2023)	Satellite based estimate of peak productivity in NE Atlantic
May–Jun 2024	48.98°N 16.36°W	41–103	This study	Total size fraction

4.2. Historic Productivity Observations

Literature estimates of integrated primary production rates for the open waters of the Northeast Atlantic are summarized in Table 3. These selected rates obtained using a variety of techniques and over different time and spatial scales indicate typical maximum rates of <150 mmol C m^{-2} d^{-1} coincident with the spring bloom, but with a range in productivity rates of 8–323 mmol C m^{-2} d^{-1}. The new estimates of primary production reported in this study compare well with these previous observations. This cross section of literature estimates is broadly encapsulated within the mean daily productivity rates derived for the North Atlantic Drift (NADR) province by Longhurst (1995) which peak in May and via the Vertically Generalized Production Model (VGPM) satellite model (Behrenfeld & Falkowski, 1997) as applied to MODIS Aqua data which peaks in June, but there can be significant interannual variability in productivity estimates around the peak timing of the spring bloom (May/June) (Figure 7). Several high productivity rates (>200 mmol C m^{-2} d^{-1}) have also been reported, which in the case of the June 2013 observations (Painter, previously unpublished) were made during a year with an unusually strong spring bloom (Figure 2).

Similarly, the new nitrate uptake rates reported here remain comparable to previous observations from the Northeast Atlantic (Table 4). We note that some of the variability shown in Table 4 derives from comparison of studies conducted across a relatively large geographical region which may experience different environmental forcings and contain different phytoplankton communities.

4.3. Interannual Variability

4.3.1. Winter Mixed Layer Depth and Seasonal Nutrient Drawdown

The winter mixed layer depth obtained from Argo floats passing through the region between 1st Jan and 1st May 2024 indicated a maximum winter mixed layer depth of 400 m but also significant spatial heterogeneity between float estimates (Figure 8; Figure S10 in Supporting Information S1). The comparison of 2024 to previous years suggests that 2024 had a shallower and later winter mixing period than previous years (Figure 8; Table S1 in

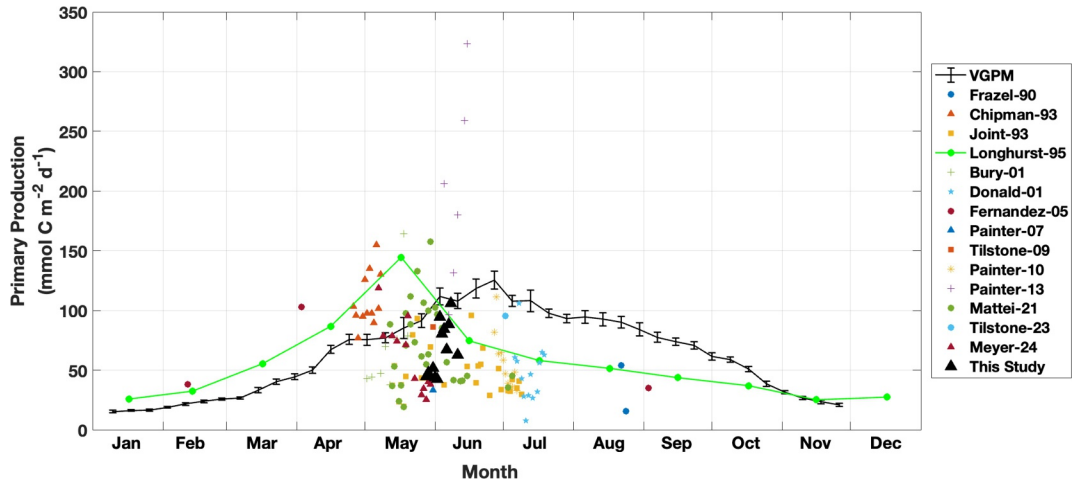

Figure 7. Selected literature estimates of primary production in the northeast Atlantic Ocean. The Longhurst-95 record (green line) is the mean annual cycle for the North Atlantic Drift Province (NADR), the VGPM record (black line; (Behrenfeld & Falkowski, 1997)) represents the mean annual cycle (2002–2020) for an area ~100 km in radius around 49°N, 16.5°W (MODIS product sourced from the Ocean Productivity site, http://orca.science.oregonstate.edu/index.php). Details of other studies listed in Table 3.

Supporting Information S1). The Argo mixed layer depth climatology of Holte et al. (2017) illustrates the long-term variability in the depth of winter mixing at the PAP-SO site which varies from 334 m (winter 2002) to 703 m (winter 2014). This climatology produces a mean winter mixed layer depth of 487 m for the period 2002–2022. Thus, a winter mixing depth of 400 m for winter 2024 is toward lower estimates and shallower than the climatological average which may have impacted pre-bloom nutrient concentrations.

4.3.2. Seasonal Nutrient Consumption

Surface nutrient concentrations in early spring, prior to bloom development, were assumed equal to nutrient concentrations at the depth of maximum winter mixing. Seasonal nutrient drawdown was calculated as the difference between these assumed winter values and the mean observed mixed layer conditions in June 2024. Six deep nutrient profiles (0–3,000 m) conducted during the cruise indicated average concentrations at 400 m of 11.7 ± 0.9 μmol NO_3^- L^{-1}, 0.7 ± 0.1 μmol PO_4^{3-} L^{-1} and 4.8 ± 0.5 μmol Si L^{-1}. Reported winter nutrient concentrations for this region are ~9 μmol NO_3^- L^{-1}, ~0.5 μmol PO_4^{3-} L^{-1}, and ~3 μmol Si L^{-1}respectively (Boyer et al., 2013; Hartman et al., 2010, 2015; Koeve, 2001). Thus, if in winter 2024 surface waters re-equilibrated with those at 400 m depth, surface nutrient conditions at the start of the growing season would have been 30%–60% higher than previously reported despite a shallower than average winter mixed layer depth.

The mean seasonal nutrient drawdown rates were 7.0 μmol NO_3^- L^{-1}, 0.41 μmol PO_4^{3-} L^{-1}, and 3.6 μmol Si L^{-1}, equating to drawdown rates of 60%, 57% and 76% of initial concentrations. This implies a significant proportion of annual nutrient consumption had already occurred prior to in situ sampling. This is only partially supported by the satellite timeseries of surface chlorophyll which shows a short lived but intense peak in chlorophyll immediately before in situ sampling commenced (Figure 2). However, this timeseries also indicates below average chlorophyll concentrations throughout March and April arguing against significant nutrient consumption. The monthly chlorophyll composites shown in Figure 3 also argue against an early bloom.

4.3.2.1. Comparison to 2023

To understand the year-to-year variability in seasonal nutrient drawdown rate we compare conditions measured 1 year earlier in May 2023 (*RRS James Cook* cruise JC247) (Gates, 2023). Surface nutrient concentrations for 8–18th May 2023 averaged 2.4 ± 0.7 μmol NO_3^- L^{-1}, 0.19 ± 0.04 μmol PO_4^{3-} L^{-1}, 2.1 ± 0.3 μmol Si L^{-1}, and 0.05 ± 0.03 μmol NH_4^+ L^{-1} and for nitrate and phosphate were lower than observed in May 2024. The maximum winter mixed layer depth in 2023 was 500 m (Figure 8), with mean nutrient concentrations at 500 m of 12.9 ± 1.7 μmol NO_3^- L^{-1}, 0.78 ± 0.1 μmol PO_4^{3-} L^{-1}, and 5.4 ± 0.8 μmol Si L^{-1}. This suggests surface nutrient concentrations could have been 1.2 μmol NO_3^- L^{-1}, 0.08 μmol PO_4^{3-}, and 0.6 μmol Si L^{-1} higher in 2023

Table 4
Selected Literature Estimates of Nitrate Uptake in the Northeast Atlantic

Sampling date	Location	Integrated NO_3^- uptake (mmol N m^{-2} d^{-1})	Reference	Notes
May 1989	46.35°N, 18.67°W	2.9	(Lowry et al., 1994; Wood, 1992)	UK BOFS study
May 1990	48.5–50°N, 17–19°W	2.5–13.6	Bury et al. (2001)	UK BOFS study
May 1990	48.5–50°N, 17–19°W	2.0–30.7	Lowry et al. (1994)	Additional UK BOFS data not in Bury et al., 2001
May–Jun 1990	47–48.5°N, 15.5–17.5°W		(Lowry et al., 1994; Wood, 1992)	UK BOFS study
Jun–Jul 1993	48.3–49.5°N, 10.5–12°W	4.0–7.4	(OMEX Project Members, 1997; OMEX Project Members and I. Joint, 2013)	OMEX-I study (multi-ship; near shelf edge)
Apr-May 1994	49.3–49.4°N, 11–13.4°W	5.5–21.0	Rees et al. (1999)	OMEX-I study (multi-ship; near shelf edge)
Sep-Oct 1995	49.0–49.7°N, 10–16.5°W	1.1–4.9	(OMEX Project Members, 1997; OMEX Project Members and I. Joint, 2013)	OMEX-II study (multi-ship; near shelf edge)
Jul 1996	37–57°N, 20°W	0.2–2.4	Donald et al. (2001)	UK Prime study
Jun 1997	42.5°N, 10.0°W	2.3	OMEX Project Members, 1997; OMEX Project Members and I. Joint 2013)	OMEX-II study (multi-ship; near shelf edge)
Jun 1998	48.5°N,9.7°W	4.0	Rees et al. (2006)	Mean value NADR province (AMT6)
Sep 2000	NADR province	0.5 ± 0.3	Varela et al. (2005)	Mean value (AMT11)
Jan–Sep 2001	38–45°N, 16–22°W	0.9–3.5	Fernandez et al. (2005)	Mean seasonal observations over annual cycle (winter to summer)
Jun 2003	47.1°N, 13.9°W	0.8	Painter et al. (2008)	12 hr photoperiod (AMT12)
May 2004	46.4–49°N, 16.4–17.3°W	8.1–13.8	Painter et al. (2007)	12 hr photoperiod (AMT14)
Jun–Jul 2006	~49°N, 16.5 W	2.0–8.0	Painter et al. (2010)	Eddy influenced
May–Jun 2024	48.98°N 16.36°W	0.8–6.6	This study	

compared to 2024 due to deeper winter mixing. By May 2023 nutrient drawdown had removed 10.45 µmol NO_3^- L^{-1} (81%), 0.59 µmol PO_4^{3-} L^{-1} (76%) and 3.3 µmol Si L^{-1} (60%). This indicated a potentially faster removal of NO_3^- and PO_4^{3-} in 2023 (~80%) compared to 2024 (~60%), but slower seasonal drawdown of Si (60% vs 76%)

Surface NO_3^- and PO_4^{3-} concentrations in May–June 2024 were higher than in May 2023, suggesting slower nutrient drawdown by the same point in the year particularly as winter 2024 starting concentrations were lower than in 2023. In contrast, surface Si concentrations were lower in May 2024 than May 2023. The slower rate of NO_3^- and PO_4^{3-} removal in 2024 is consistent with the satellite surface chlorophyll record which showed a weaker than average bloom (Figure 3) and may reflect interannual differences in winter mixing intensity and timing (Figure 8) or to changes in the phytoplankton community. The resulting stoichiometry (N:Si:P) of the nutrient drawdown in 2023 was 17.6:5.5:1 whereas in 2024 it was 17.3:8.9:1. The comparatively faster drawdown of Si in spring 2024 is not obviously explained but may be due to overestimation of the initial winter 2024 starting concentration, or to a difference in the phytoplankton community between years.

4.4. Surface Ocean Circulation

To better understand the history of waters sampled in May and June 2024 the trajectories of Lagrangian drifters from the global drifter program were examined (Lumpkin & Centurioni, 2019). For the region 40–60°N, 5–36°W and for the time period 1 June 2023 to 1 June 2024 8 drifters were identified that passed within 25 km of the nominal sampling location with a further two drifters that traversed the region to the north of the sampling site

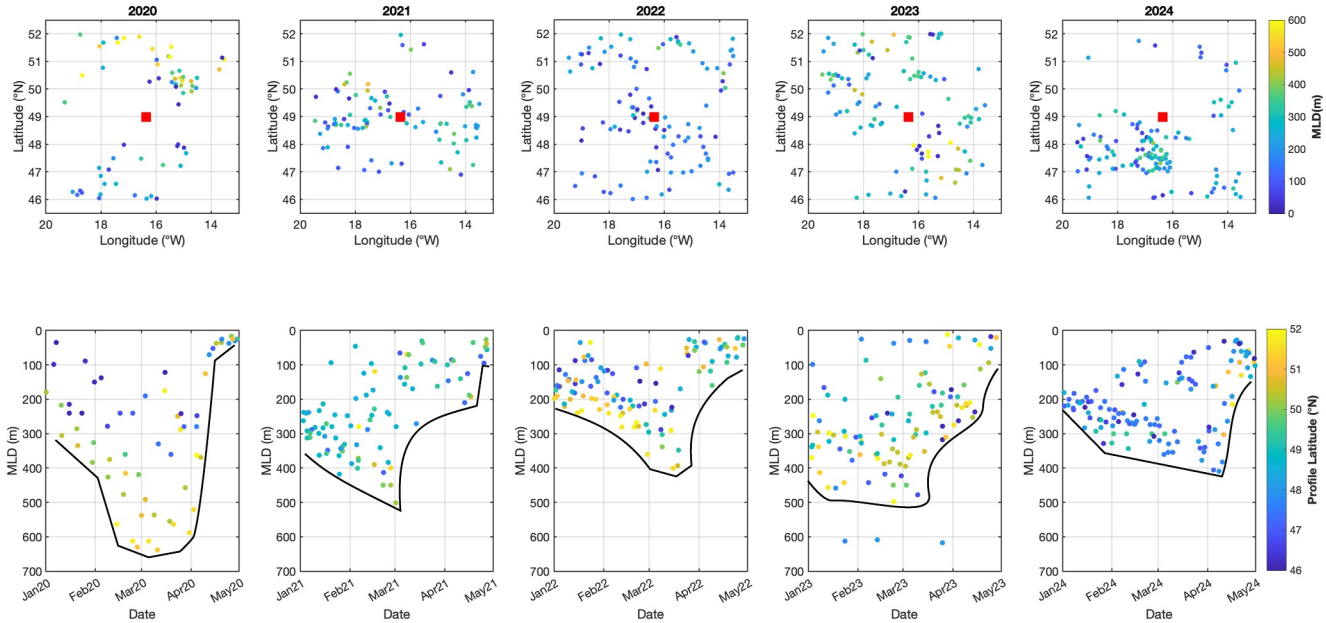

Figure 8. Argo float based estimates of mixed layer depths for the period 1st Jan to 30th April for years 2020–2024. Upper plots show float profile positions and are colored by the mixed layer depth. Lower plots show the temporal evolution of mixed layer depth. The black line is for illustrative purposes to highlight the year-to-year variation in maximum depth and timing of maximum depth of winter mixing.

(Figure 9). Drifter trajectories indicated a common eastward movement along comparable pathways with floats passing to the south of our sampling site heading toward the Bay of Biscay and floats passing to the north heading toward Ireland. These displacements were in keeping with prevailing westerly winds and several floats ultimately grounded along regional shorelines. Not all drifters persisted within the region for the full time period and horizontal displacements differed markedly between individual floats. For example, float WMO1801678 moved ∼1,600 km between 1 Jan 2024 and 1 June 2024 passing directly through our sampling site implying that surface waters sampled in May and June 2024 were likely sourced from a remote western origin. In contrast float WMO 4101656 moved only 380 km in the same period remaining <270 km from our sampling location for ∼6 months implying a more localized origin for the sampled waters. Only four floats (WMO 4101656; 4402735; 4402881 and 6202597) provided adequate temporal coverage to estimate a likely origin and with the exception of WMO 4101656 indicated displacement distances of ∼1,100–1,600 km thus making a remote western origin more likely.

The surface drifter results were consistent with Lagrangian particle tracking experiments using a forced ocean model (Text S3 in Supporting Information S1). These model results not only showed similar North Atlantic circulatory features during spring 2024 that compared well to recent years (Figure S11 in Supporting Information S1), but also indicated that wider North Atlantic circulatory pathways in the year preceding spring 2024 were consistent with previous years (Figures S12–S14 in Supporting Information S1). These latter results rule out a southern origin for the waters sampled in May 2024 and suggest that observed conditions were instead the result of regional forcings rather than being imported into the region.

4.5. Thermal Preconditioning of the 2024 Spring Bloom

Since April 2023 global sea surface temperatures have been significantly elevated above historic ranges (Terhaar et al., 2025). For the North Atlantic region temperatures have been over 1°C warmer than historic records (Climate Reanalyzer, 2025) and in 2023 widespread warming led to an intense but ultimately short-lived marine heatwave in the eastern North Atlantic (Berthou et al., 2024; Carton et al., 2025; England et al., 2025; Jacobs et al., 2024; McCarthy et al., 2023). Waters to the west of Ireland were impacted by a Category IV marine heatwave in June 2023 (Hobday et al., 2016, 2018; NOAA Coral Reef Watch, 2021) at which time the sea surface temperature anomaly exceeded 4°C above the long-term (1983–2012) 90th percentile SST (Jacobs et al., 2024). Whilst this heatwave was intense and unusual for the region it was also short lived (2 weeks) with only minor impacts on surface chlorophyll reported (Jacobs et al., 2024). Elevated sea surface temperatures were however

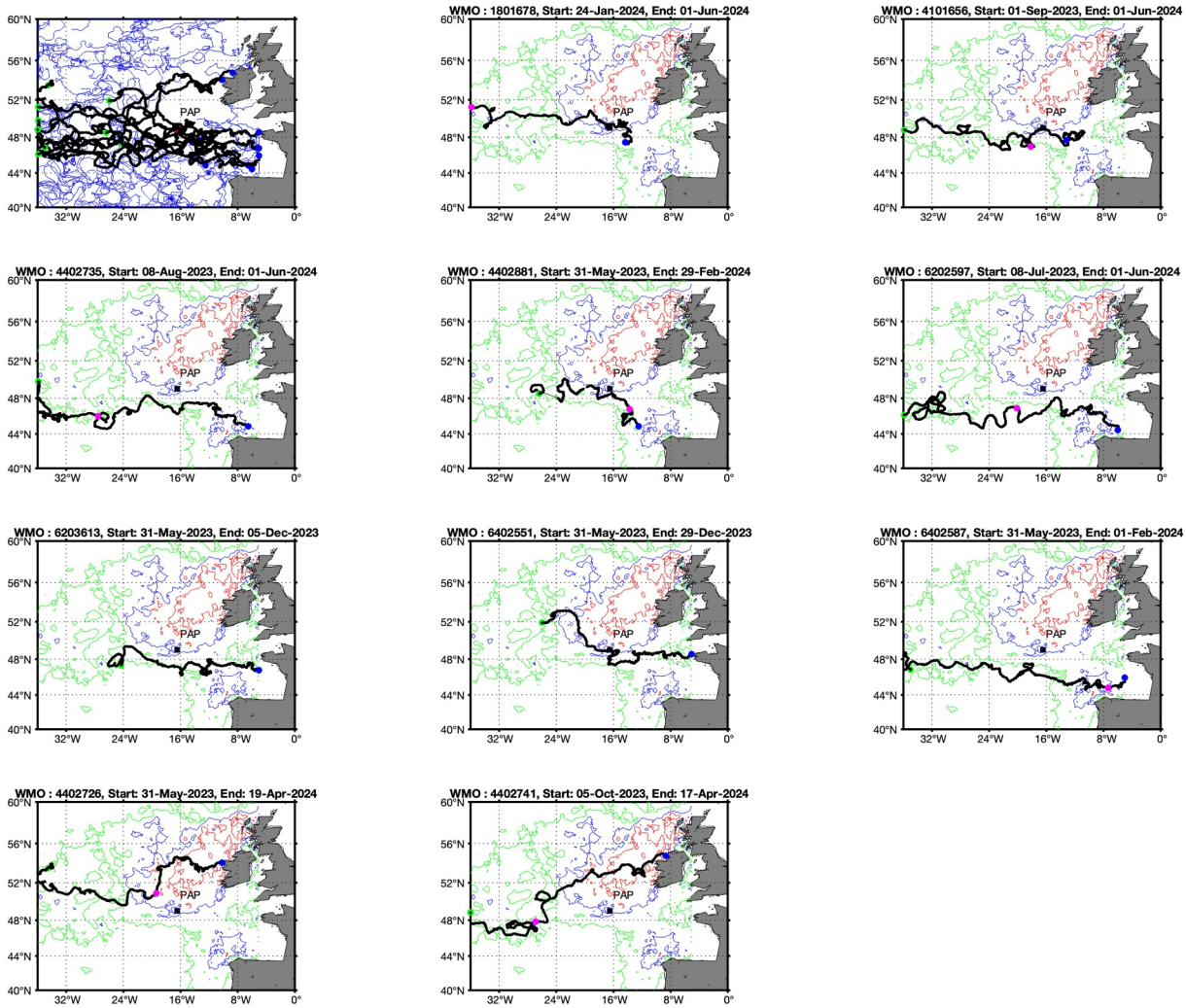

Figure 9. Trajectory plots of selected surface drifter floats passing within 25 km of this study's sampling site (indicated by the black square). The upper map shows all float trajectories within the space and time constraints (blue lines) with key selected floats highlighted in black. Separate subplots show the individual float trajectories for the selected floats (black lines) along with contours indicating the extent and severity of the 2023 marine heat wave on 20 June 2023. In all subplots the initial float positions are indicated by the green circles, the final position by the blue circles and where possible the float position on 1 Jan 2024 is indicated by the pink circles. Marine heat wave contours designate waters impacted by category II (green), category III (blue) and category IV (red) sea surface temperature anomalies. WMO ID number and dates of deployment indicated above each subplot. Data accessed via https://www.aoml.noaa.gov/phod/gdp/interpolated/data/all.php (last access 26 Feb 2025).

recorded across a much wider area of the North Atlantic and over several months (Carton et al., 2025). The MHW classification scheme of Hobday et al. (2018) suggests that category II and occasionally category III conditions would have impacted those waters that ultimately reached our sampling site in spring 2024 (Figure 9).

The longer-term year-to-year consequences of marine temperature anomalies on subsequent regional marine productivity however remain unclear due to the intervening period of seasonal cooling and deep winter convective mixing which resets water column temperatures. Yet despite seasonal cooling both global temperatures and North Atlantic temperatures during boreal winter 2024 remained high relative to long term records (Climate Reanalyzer, 2025; Terhaar et al., 2025). Convective mixing in winter 2024 was shallower and later than normal compared to recent years (Figure 8) suggesting changes to stratification intensity.

Sampling in spring 2024 occurred following an extended and unusual period of elevated temperatures which included widespread surface temperature anomalies between January and March (Figure S3 in Supporting Information S1). Whilst the intense heat wave west of Ireland in 2023 is unlikely to have directly preconditioned the phytoplankton community or the waters that subsequently fueled the 2024 spring bloom, spatially more extensive

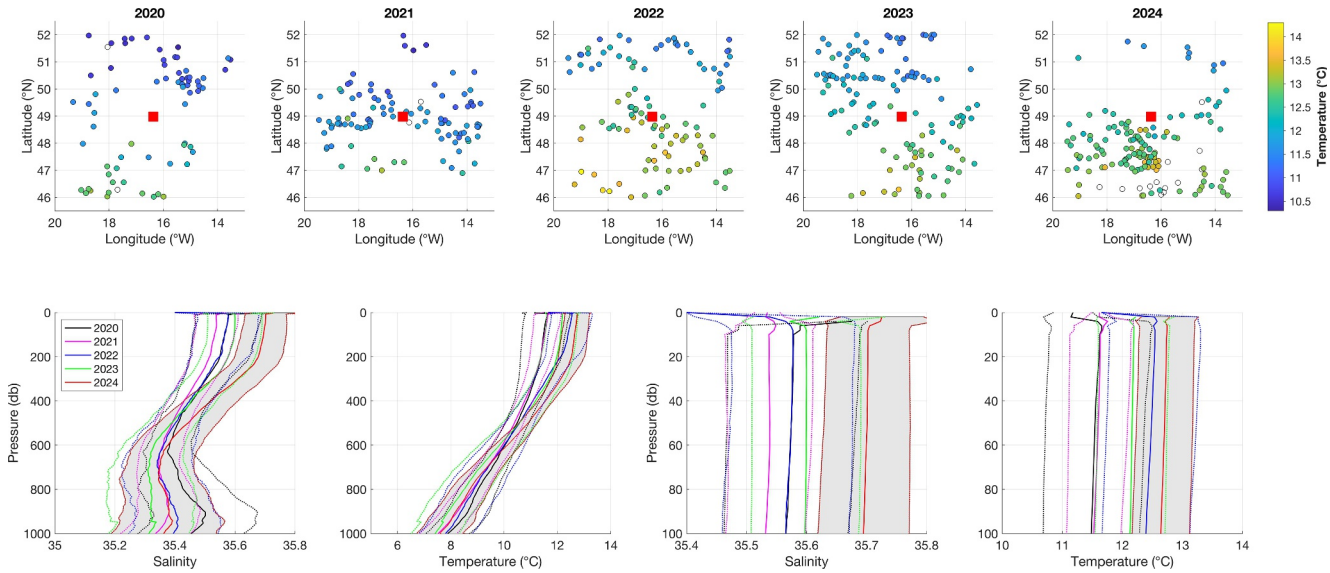

Figure 10. Argo float based assessment of the mean ocean temperature and salinity between 1st Jan–30th Apr for the years 2020–2024. Upper maps show positions of all Argo float profiles identified within ±3° of the study site, and the mean surface (0–10 m) temperature. The red square indicates the nominal position of this study. The lower plots show (left) the mean 0–1,000 m and (right) 0–100 m profiles of temperature and salinity (solid lines) along with standard deviation of the mean (dashed lines) for each year. Gray shading highlights the standard deviation for conditions during 2024.

but less severe warming across remote western waters and specifically prolonged warming of the wider North Atlantic during winter 2024 may have. Li et al. (2024) found that anomalous winter warming in the NW Mediterranean Sea led to reductions in phytoplankton carbon biomass of up to 70% and reductions in productivity of up to 80% during the subsequent spring bloom; magnitudes comparable to the reductions in productivity and biomass concentrations reported here. It was also reported by Li et al. (2024) that warming increased water transparency due to a shift toward smaller phytoplankton cells. Anomalously low irradiance attenuation coefficients were a characteristic of our early sampling thus anecdotally implying shifts within the phytoplankton community.

4.5.1. Thermal History of the Northeast Atlantic

The mean seasonal surface (0–10 m) temperature and salinity for 2020–2024 ranged from 11.47 ± 0.24°C to 12.75 ± 0.03°C and 35.538 ± 0.068 to 35.712 ± 0.012 g kg^{-1} with conditions in winter 2024 warmer and more saline than previous years (Table S1 in Supporting Information S1). The mean temperature in 2024 was more than 0.3°C warmer than the next warmest year (2022; coincidentally another year with shallow winter mixing Figure 8), whilst salinity was higher by ∼0.1 compared to 2020. Elevated surface temperatures compared to climatological conditions were also evident between January and March in satellite SST data (Figure S3 in Supporting Information S1). Lagrangian model results reveal no unusual circulatory pathways in the year prior to June 2024 (Figure S11 in Supporting Information S1), implying that the observed conditions were the result of local forcings rather than being due to an influx of waters from a southern or subtropical location. The mean temperature and salinity profiles demonstrate 2024 was warmer and more saline than previous years, particularly within the upper 100 m (Figure 10). Strong persistent thermal anomalies related to significant warming of the North Atlantic throughout 2023 and 2024 may therefore have contributed to the formation of a large low productivity region in the Northeast Atlantic in 2024.

5. Conclusions

An extensive and persistent region of low chlorophyll concentrations was identified in the northeast Atlantic throughout 2024 from satellite data and in situ sampling. A warm winter preceded the 2024 spring bloom with weaker than average winter mixing. Our results suggest that weak mixing, following a period of prolonged North Atlantic warming may have led directly to a weaker spring bloom. In situ measurements timed to coincide with the peak of the annual spring bloom sampled the southern edge of this feature where surface Chl-a concentrations of

~0.2–0.3 μg L^{-1} were less than half of concentrations observed across the wider North Atlantic region (~0.5 μg L^{-1}), and around one-quarter of concentrations considered typical for the spring bloom period. Initial environmental conditions indicated (a) relatively deep mixed layer depths (60–80m), (b) weak vertical gradients in temperature, salinity and Chl-a, and (c) optically clear water with Kd of 0.05–0.07 (unusually low for the region where 0.1 is more typical). Despite conditions appearing comparable to the late winter period, surface nutrients were potentially reduced by 60%–76% compared to estimated winter maximum concentrations yet measurements of net primary production (0.5–0.6 g C m^{-2} d^{-1}), new production (0.08–0.13 g C m^{-2} d^{-1}) and nitrate uptake (0.8–1.3 mmol N m^{-2} d^{-1}) were between 2 and 5-fold lower than found in surrounding waters. The persistence of this region of low productivity across the Northeast Atlantic for several months, and the limited availability of opal as a key ballast mineral is likely to have had implications for carbon export fluxes derived from the 2024 spring bloom.

Conflict of Interest

The authors declare no conflicts of interest relevant to this study.

Data Availability Statement

All cruise data described in this study have been submitted to the British Oceanographic Data Centre (www.bodc.ac.uk) and are available through the BODC Published Data Library (https://www.bodc.ac.uk/data/published_data_library/) via Painter et al. (2025). Data may also be requested via the corresponding author. Modis Aqua data products (chlorophyll-a, sea surface temperature and particulate inorganic carbon) at 8-day and monthly temporal resolution were obtained from the NASA Ocean Biology Distributed Active Archive Centre (OB.DAAC) via https://oceandata.sci.gsfc.nasa.gov/l3/ Argo float data were collected and made freely available by the International Argo Program and the national programs that contribute to it (https://argo.ucsd.edu, https://www.ocean-ops.org). The Argo Program is part of the Global Ocean Observing System. Argo data were obtained via the international Global Data Assembly Centres (https://data-argo.ifremer.fr & https://usgodae.org/pub/outgoing/argo). Surface drifter data were obtained from the Global Drifter Programme (https://www.aoml.noaa.gov/phod/gdp/index.php) via the NOAA ERDAP server (https://erddap.aoml.noaa.gov/gdp/erddap/tabledap/drifter_6hour_qc.html).

Acknowledgments

We thank the UK Natural Environment Research Council for funding through its National Capability Long-term Single Centre Science Programme, Atlantic Climate and Environmental Strategic Science (**AtlantiS**; https://projects.noc.ac.uk/atlantis/) under Grant NE/Y005589/1. As part of the **AtlantiS** project (2024–2029), the National Oceanography Centre is developing a suite of global ocean model configurations to perform multi-decadal simulations which extend to Nea-Present Day. The Joint Marine Modelling Programme (JMMP) is a partnership between the UK Met Office and UK research centres: the National Oceanography Centre, the British Antarctic Survey and the Centre for Polar Observation and Modelling (https://www.metoffice.gov.uk/research/approach/collaboration/joint-marine-modelling-programme). This work used the ARCHER2 UK National Supercomputing Service (https://www.archer2.ac.uk). Additional financial support was provided through the EU MINKE project via transnational access (Minke – Metrology for Integrated marine maNagement and Knowledge-transfer nEtwork). MINKE received funding from the European Union's Horizon 2020 research and innovation program under Grant agreement 101008724. The authors thank the NERC Earth Observation Data Analysis and AI Service (NEODAAS; www.neodaas.ac.uk) for supplying data for this study (Figures S1–S3 in Supporting Information S1). B. Hambach and M. Wilding (University of Southampton) are thanked for elemental and isotopic analysis. We thank the captain and crew of the *RRS James Cook* for their efforts on research cruise JC263.

References

Argo. (2000). *Argo float data and metadata from global data assembly centre (Argo GDAC)*. SEANO.

Asch, R. G. (2019). In A. M. Cisneros-Montemayor, W. W. I. Cheung, & Y. Ota (Eds.), *Changing seasonality of the sea: Past, present and future in predicting future oceans*. Elsevier.

Balch, W. M., Gordon, H. R., Bowler, B. C., Drapeau, D. T., & Booth, E. S. (2005). Calcium carbonate measurements in the surface global ocean based on moderate-resolution imaging spectroradiometer data. *Journal of Geophysical Research*, *110*(C7), C07001. https://doi.org/10.1029/2004jc002560

Becker, S., Aoyama, M., Woodward, E. M. S., Bakker, K., Coverly, S., Mahaffey, C., & Tanhua, T. (2020). GO-SHIP repeat hydrography nutrient manual: The precise and accurate determination of dissolved inorganic nutrients in seawater, using continuous flow analysis methods. *Frontiers in Marine Science*, *7*, 581790. https://doi.org/10.3389/fmars.2020.581790

Behrenfeld, M. J., & Falkowski, P. G. (1997). Photosynthetic rates derived from satellite-based chlorophyll concentration. *Limnology & Oceanography*, *42*(1), 1–20. https://doi.org/10.4319/lo.1997.42.1.0001

Berthou, S., Renshaw, R., Smyth, T., Tinker, J., Grist, J. P., Wihsgott, J. U., et al. (2024). Exceptional atmospheric conditions in June 2023 generated a northwest European marine heatwave which contributed to breaking land temperature records. *Communications Earth & Environment*, *5*(1), 287. https://doi.org/10.1038/s43247-024-01413-8

Boyer, T. P., Antonov, J. I., Baranova, O. K., Coleman, C., Garcia, H. E., Grodsky, A., et al. (2013). *World ocean database 2013. NOAA atlas NESDIS 72* (Ed.), S. Levitus, & A. Mishonov (Technical Ed.), (p. 209). https://doi.org/10.7289/V5NZ85MT

Bury, S. J., Boyd, P. W., Preston, T., Savidge, G., & Owens, N. J. P. (2001). Size-fractionated primary production and nitrogen uptake during a North Atlantic phytoplankton bloom: Implications for carbon export estimates. *Deep-Sea Research Part I*, *48*(3), 689–720. https://doi.org/10.1016/s0967-0637(00)00066-2

Carton, J. A., Chepurin, G. A., Hackert, E. C., & Huang, B. (2025). Remarkable 2023 North Atlantic Ocean warming. *Geophysical Research Letters*, *52*(3), e2024GL112551. https://doi.org/10.1029/2024gl112551

Chapman, P., & Mostert, S. A. (1990). Does freezing of nutrient samples cause analytical errors? *South African Journal of Marine Science*, *9*(1), 239–247. https://doi.org/10.2989/025776190784378763

Chipman, D. W., Marra, J., & Takahashi, T. (1993). Primary production at 47*N and 20*W in the North Atlantic Ocean: A comparison between the ^{14}C incubation method and the mixed layer carbon budget. *Deep-Sea Research II*, *40*(1/2), 151–169. https://doi.org/10.1016/0967-0645(93)90011-b

Climate Reanalyzer. (2025). Daily Sea Surface Temperature (North Atlantic). Climate Change Institute, University of Maine. Retrieved from https://climatereanalyser.org

Coplen, T. B. (1994). Reporting of stable hydrogen, carbon, and oxygen isotopic abundances. *Pure and Applied Chemistry*, *66*(2), 273–276. https://doi.org/10.1351/pac199466020273

Coplen, T. B., Krouse, H. R., & Bohlke, J. H. (1992). Reporting of nitrogen-isotope abundances. *Pure and Applied Chemistry*, *64*(6), 907–908. https://doi.org/10.1351/pac199264060907

Cornec, M., Claustre, H., Mignot, A., Guidi, L., Lacour, L., Poteau, A., et al. (2021). Deep chlorophyll maxima in the global ocean: Occurrences, drivers and characteristics. *Global Biogeochemical Cycles*, *35*(4), e2020GB006759. https://doi.org/10.1029/2020gb006759

Daniels, C. J., Tyrrell, T., Poulton, A. J., & Pettit, L. (2012). The influence of lithogenic material on particulate inorganic carbon measurements of coccolithophores in the Bay of Biscay. *Limnology & Oceanography*, *57*(1), 145–153. https://doi.org/10.4319/lo.2012.57.1.0145

de Boyer Montegut, C., Madec, G., Fischer, A. S., Lazar, A., & Ludicone, D. (2004). Mixed layer depth over the global ocean: An examination of profile data and a profile-based climatology. *Journal of Geophysical Research*, *109*(C12), C12003. https://doi.org/10.1029/2004jc002378

Diaz-Rosas, F., Vargas, C. A., & von Dassow, P. (2025). Particulate inorganic carbon pools by coccolithophores in low oxygen/low pH waters off the Southeast Pacific margin. *Biogeosciences*, *22*(17), 4405–4422. https://doi.org/10.5194/bg-22-4405-2025

Donald, K. M., Joint, I., Rees, A. P., Woodward, E. M. S., & Savidge, G. (2001). Uptake of carbon, nitrogen and phosphorus by phytoplankton along the 20 degrees W Meridian in the NE Atlantic between 57.5 degrees N and 37 degrees N. *Deep-Sea Research Part II*, *48*(4–5), 873–897. https://doi.org/10.1016/s0967-0645(00)00102-8

Dore, J. E., Houlihan, T., Hebel, D. V., Tien, G., Tupas, L., & Karl, D. M. (1996). Freezing as a method of sample preservation for the analysis of dissolved inorganic nutrients in seawater. *Marine Chemistry*, *53*(3–4), 173–185. https://doi.org/10.1016/0304-4203(96)00004-7

Dugdale, R. C., & Goering, J. J. (1967). Uptake of new and regenerated forms of nitrogen in primary productivity. *Limnology & Oceanography*, *12*(2), 196–206. https://doi.org/10.4319/lo.1967.12.2.0196

England, M. H., Li, Z., Huguenin, M. F., Kiss, A. E., Sen Gupta, A., Holmes, R. M., & Rahmstorf, S. (2025). Drivers of the extreme North Atlantic marine heatwave during 2023. *Nature*, *642*(8068), 636–643. https://doi.org/10.1038/s41586-025-08903-5

Fernandez, C., Raimbault, P., Garcia, N., Rimmelin, P., & Caniaux, G. (2005). An estimation of annual new production and carbon fluxes in the northeast Atlantic Ocean during 2001. *Journal of Geophysical Research*, *110*, C07S13. https://doi.org/10.1029/2004JC002616

Follows, M., & Dutkiewicz, S. (2002). Meterorological modulations of the North Atlantic spring bloom. *Deep-Sea Research Part II*, *49*, 321–344.

Frazel, D. W., & Berberian, G. (1990). Distributions of chlorophyll and primary productivity in relation to water column structure in the eastern North Atlantic Ocean. *Global Biogeochemical Cycles*, *4*(3), 241–251. https://doi.org/10.1029/gb004i003p00241

Friedland, K. D., Nielsen, J. M., Record, N. R., Brady, D. C., & Morrow, C. J. (2024). The phenology of the spring phytoplankton bloom in the North Atlantic does not trend with temperature. *Elementa: Science of the Anthropocene*, *12*(1), 00111. https://doi.org/10.1525/elementa.2023.00111

Friedland, K. D., Record, N. R., Asch, R. G., Kristiansen, T., Saba, V. S., Drinkwater, K. F., et al. (2016). Seasonal phytoplankton blooms in the North Atlantic linked to the overwintering strategies of copepods. *Elementa Science of the Anthropocene*, *4*, 000099. https://doi.org/10.12952/journal.elementa.000099

Gao, Z., Jiang, Y., He, J., Wu, J., & Christakos, G. (2023). Comparing eight remotely sensed sea surface temperature products and Bayesian maximum entropy-based data fusion products. *Spatial Statistics*, *54*, 100741. https://doi.org/10.1016/j.spasta.2023.100741

Gates, A. R. (2023). *RRS James cook cruise 247: Multidecadal research at the porcupine abyssal plain 5–-22 May 2023 (national oceanography Centre research expedition report, No. 76)*. National Oceanography Centre, (p. 199).

GilpinDavidson, L. C. K., & Roberts, E. (2004). The influence of changes in nitrogen: Silicon ratios on diatom growth dynamics. *Journal of Sea Research*, *51*(1), 21–35. https://doi.org/10.1016/j.seares.2003.05.005

Good, S., Fiedler, E., Mao, C., Martin, M. J., Maycock, A., Reid, R., et al. (2020). The current configuration of the OSTIA system for operational production of foundation sea surface temperature and ice concentration analyses. *Remote Sensing*, *12*(4), 720. https://doi.org/10.3390/rs12040720

Gordon, H. R., Boynton, G. C., Balch, W. M., Groom, S. B., Harbour, D. S., & Smyth, T. J. (2001). Retrieval of coccolithophore calcite concentration from SeaWiFS imagery. *Geophysical Research Letters*, *28*(8), 1587–1590. https://doi.org/10.1029/2000gl012025

Green, D. R. H., Cooper, M. J., German, C. R., & Wilson, P. A. (2003). Optimization of an inductively coupled plasma—Optical emission spectrometry method for the rapid determination of high-precision Mg/Ca and Sr/Ca in foraminiferal calcite. *Geochemistry, Geophysics, Geosystems*, *4*(6), 8404. https://doi.org/10.1029/2002gc000488

Guan, L., & Kawamura, H. (2003). SST availabilities of satellite infrared and microwave measurements. *Journal of Oceanography*, *59*(2), 201–209. https://doi.org/10.1023/a:1025543305658

Guinaldo, T., & Neukermans, G. (2025). *Exceptional 2023 marine heat wave reshapes North Atlantic coccolithophore blooms*. EGUsphere. https://doi.org/10.5194/egusphere-2025-1862

Hama, T., Miyazaki, T., Ogawa, Y., Iwakuma, T., Takahashi, M., Otsuki, A., & Ichimura, S. (1983). Measurement of photosynthetic production of marine phytoplankton population using a stable ^{13}C isotope. *Marine Biology*, *73*(1), 31–36. https://doi.org/10.1007/bf00396282

Hartman, S. E., Bett, B. J., Durden, J. M., Henson, S. A., Iversen, M., Jeffreys, R. M., et al. (2021). Enduring science: Three decades of observing the Northeast Atlantic from the porcupine abyssal plain sustained observatory (PAP-SO). *Progress in Oceanography*, *191*, 102508. https://doi.org/10.1016/j.pocean.2020.102508

Hartman, S. E., Jiang, Z. P., Turk, D., Lampitt, R. S., Frigstad, H., Ostle, C., & Schuster, U. (2015). Biogeochemical variations at the porcupine abyssal plain sustained observatory in the northeast Atlantic Ocean, from weekly to inter-annual timescales. *Biogeosciences*, *12*(3), 845–853. https://doi.org/10.5194/bg-12-845-2015

Hartman, S. E., Lampitt, R. S., Larkin, K. E., Pagnani, M., Campbell, J., Gkritzalis, T., et al. (2012). The porcupine abyssal plain fixed-point sustained observatory (PAP-SO): Variations and trends from the Northeast Atlantic fixed-point time-series. *ICES Journal of Marine Science*, *69*(5), 776–783. https://doi.org/10.1093/icesjms/fss077

Hartman, S. E., Larkin, K. E., Lampitt, R. S., Lankhorst, M., & Hydes, D. J. (2010). Seasonal and inter-annual biogeochemical variations in the porcupine abyssal plain 2003–2005 associated with winter mixing and surface circulation. *Deep-Sea Research Part II*, *57*(15), 1303–1312. https://doi.org/10.1016/j.dsr2.2010.01.007

Hemsley, V. S., Smyth, T. J., Martin, A. P., Frajka-Williams, E., Thompson, A. F., Damerell, G., & Painter, S. C. (2015). Estimating Oceanic primary production using vertical irradiance and chlorophyll profiles from ocean gliders in the North Atlantic. *Environmental Science & Technology*, *49*(19), 11612–11621. https://doi.org/10.1021/acs.est.5b00608

Hobday, A. J., Alexander, L. V., Perkins, S. E., Smale, D. A., Straub, S. C., Oliver, E. C. J., et al. (2016). A hierarchical approach to defining marine heatwaves. *Progress in Oceanography*, *141*, 227–238. https://doi.org/10.1016/j.pocean.2015.12.014

Hobday, A. J., Oliver, E. C. J., Gupta, A. S., Benthuysen, J. A., Burrows, M. T., Donat, M. G., et al. (2018). Categorizing and naming marine heatwaves. *Oceanography*, *31*(2). https://doi.org/10.5670/oceanog.2018.205

Holte, J., Talley, L. D., Gilson, J., & Roemmich, D. (2017). An Argo mixed layer climatology and database. *Geophysical Research Letters*, *44*(11), 5618–5626. https://doi.org/10.1002/2017gl073426

Hu, C., Feng, L., Lee, Z., Franz, B. A., Bailey, S. W., Werdell, P. J., & Proctor, C. W. (2019). Improving satellite global chlorophyll a data products through algorithm refinement and data recovery. *Journal of Geophysical Research: Oceans*, *124*(3), 1524–1543. https://doi.org/10.1029/2019jc014941

Huang, B., Liu, C., Banzon, V., Freeman, E., Graham, G., Hankins, B., et al. (2021). Improvements of the daily optimum interpolation sea surface temperature (DOISST) version 2.1. *Journal of Climate*, *34*(8), 2923–2939. https://doi.org/10.1175/jcli-d-20-0166.1

IOCCG, Balch, W. M., Carranza, M., Cetinic, I., Chaves, J. E., Duhamel, S., et al. (2022). Aquatic primary productivity field protocols for satellite validation and model synthesis. In R. A. Vandermeulen & J. E. Chaves (Eds.), *IOCCG ocean optics and biogeochemistry protocols for satellite ocean colour Sensor validation* (Vol. 7.0). Dartmouth, NS, Canada, International Ocean Colour Coordinating Group.202.

Jacobs, Z. L., Jebri, F., Wakelin, S., Strong, J., Popova, E., Srokosz, M., & Loveridge, A. (2024). Marine heatwaves and cold spells in the Northeast Atlantic: What should the UK be prepared for? *Frontiers in Marine Science*, *11*, 1434365. https://doi.org/10.3389/fmars.2024.1434365

Joint, I., Pomroy, A., Savidge, G., & Boyd, P. (1993). Size-fractionated primary productivity in the northeast Atlantic in May–July 1989. *Deep-Sea Research Part II*, *40*(1/2), 423–440. https://doi.org/10.1016/0967-0645(93)90025-i

Karl, D. M., Dore, J. E., Hebel, D. V., & Winn, C. (1991). Procedures for particulate carbon nitrogen, phosphorus and total mass analyses used in the US-JGOFS Hawaii ocean time-series program. In D. C. Hurd & D. W. Spencer (Eds.), *Marine particles: Analysis and characterization* (pp. 71–77). American Geophysical Union.

Kelly, S., Popova, E., Yool, A., Jebri, F., Oliver, S., & Srokosz, M. (2025). Abrupt changes in the timing and magnitude of the North Atlantic bloom over the 21st century. *Journal of Geophysical Research: Oceans*, *130*(3), e2024JC022284. https://doi.org/10.1029/2024jc022284

Kennedy, P., Kennedy, H., & Papadimitriou, S. (2005). The effect of acidification on the determination of organic carbon, total nitrogen and their stable isotopic composition in algae and marine sediment. *Rapid Communications in Mass Spectrometry*, *19*(8), 1063–1068. https://doi.org/10.1002/rcm.1889

Kilpatrick, K. A., Podestá, G., Walsh, S., Williams, E., Halliwell, V., Szczodrak, M., et al. (2015). A decade of sea surface temperature from MODIS. *Remote Sensing of Environment*, *165*, 27–41. https://doi.org/10.1016/j.rse.2015.04.023

Koeve, W. (2001). Wintertime nutrients in the North Atlantic—New approaches and implications for new production estimates. *Marine Chemistry*, *74*(4), 245–260. https://doi.org/10.1016/s0304-4203(01)00016-0

Leblanc, K., Hare, C. E., Feng, Y., Berg, G. M., DiTullio, G. R., Neely, A., et al. (2009). Distribution of calcifying and silicifying phytoplankton in relation to environmental and biogeochemical parameters during the late stages of the 2005 North East Atlantic spring bloom. *Biogeosciences*, *6*(10), 2155–2179. https://doi.org/10.5194/bg-6-2155-2009

Leblanc, K., Leynaert, A., Fernandez, C. I., Rimmelin, P., Moutin, T., Raimbault, P., et al. (2005). A seasonal study of diatom dynamics in the North Atlantic during the POMME experiment (2001): Evidence for Si limitation of the spring bloom. *Journal of Geophysical Research*, *110*, C07S14. https://doi.org/10.1029/2004JC002621

Li, M., Organelli, E., Serva, F., Bellacicco, M., Landolfi, A., Pisano, A., et al. (2024). Phytoplankton spring bloom inhibited by marine heatwaves in the north-western Mediterranean Sea. *Geophysical Research Letters*, *51*(20), e2024GL109141. https://doi.org/10.1029/2024gl109141

Longhurst, A. (1995). Seasonal cycles of pelagic production and consumption. *Progress in Oceanography*, *36*(2), 77–167. https://doi.org/10.1016/0079-6611(95)00015-1

Longhurst, A. (1998). *Ecological geography of the sea*. Academic Press.

Lowry, R. K., Machin, P., & Cramer, R. N. (1994). *BOFS North Atlantic data set. Oceanographic data collected during the North Atlantic cruises of the NERC biogeochemical ocean flux study (1989–1991): A UK contribution of JGOFS*. B. O. D. C. Natural Environmental Research Council.

Lumpkin, R., & Centurioni, L. (2019). *Global drifter program quality-controlled 6-hour interpolated data from ocean surface drifting buoys [buoydata_15001_current]*. NOAA National Centers for Environmental Information. https://doi.org/10.25921/7ntx-z961

Marañón, E. (2005). Phytoplankton growth rates in the Atlantic subtropical gyres. *Limnology & Oceanography*, *50*(1), 299–310.

Martinez, E., Antoine, D., D'Ortenzio, F., & de Boyer Montegut, C. (2011). Phytoplankton spring and fall blooms in the North Atlantic in the 1980s and 2000s. *Journal of Geophysical Research*, *116*, C11029. https://doi.org/10.1029/2010JC006836

Mattei, F., & Scardi, M. (2021). Collection and analysis of a global marine phytoplankton primary-production dataset. *Earth System Science Data*, *13*(10), 4967–4985. https://doi.org/10.5194/essd-13-4967-2021

McCarthy, G. D., Plecha, S., Charria, G., Simon, A., Poppeschi, C., & Russo, A. (2023). The marine heatwave west of Ireland in June 2023. *Weather*, *78*(11), 321–323. https://doi.org/10.1002/wea.4498

Meyer, M. G., Brzezinski, M. A., Cohn, M. R., Kramer, S. J., Paul, N., Sharpe, G., et al. (2024). Size-fractionated primary production dynamics during the decline phase of the North Atlantic spring bloom. *Global Biogeochemical Cycles*, *38*(7), e2023GB008019. https://doi.org/10.1029/2023gb008019

Mitchell, C., & Godrijan, J. (2025). Particulate inorganic carbon in the ocean: Evaluation of discrete sampling protocols. *Limnology and Oceanography: Methods*, *23*(5), 326–335. https://doi.org/10.1002/lom3.10683

Mitchell, C., Hu, C., Bowler, B., Drapeau, D., & Balch, W. M. (2017). Estimating particulate inorganic carbon concentrations of the global ocean from ocean color measurements using a reflectance difference approach. *Journal of Geophysical Research: Oceans*, *122*(11), 8707–8720. https://doi.org/10.1002/2017jc013146

Morán, X. A. G., López-Urrutia, Á., Calvo-Diaz, A., & Li, W. K. W. (2010). Increasing importance of small phytoplankton in a warmer ocean. *Global Change Biology*, *16*(3), 1137–1144.

NOAA Coral Reef Watch. (2021). NOAA marine heatwave watch version 1.0.1 daily global 5km satellite marine heatwave product [Dataset]. Retrieved from https://coralreefwatch.noaa.gov/product/marine_heatwave/CollegePark,Maryland,USA,NOAACoralReefWatch

OMEX Project Members. (1997). Ocean margin exchange, OMEX-I project dataset (1993–1996). *Bidston Observatory, Birkenhead, Merseyside (2 CD-ROM), hdl:10013/epic.28817.d001*. Natural Environmental Research Council published by British Oceanographic Data Center.

OMEX Project Members, & Joint, I. (2013). *Uptake rates during VALDIVIA cruise VA137*. PANGAEA. https://doi.org/10.1594/PANGAEA.807421

Painter, S. C., Feltham, C., Muliawan, R. E., Mawji, E., & Peel, K. (2025). Primary production, nitrate uptake, particulate and chlorophyll biomass in the Northeast Atlantic during RRS James cook cruise JC263 in spring 2024. *NERC EDS British Oceanographic Date Centre, NOC*. https://doi.org/10.5285/3b9d26a0-17f1-bc3d-e063-7086abc097fb

Painter, S. C., Finlay, M., Hemsley, V. S., & Martin, A. P. (2016). Seasonality, phytoplankton succession and the biogeochemical impacts of an autumn storm in the northeast Atlantic Ocean. *Progress in Oceanography*, *142*, 72–104. https://doi.org/10.1016/j.pocean.2016.02.001

Painter, S. C., Lucas, M. I., Stinchcombe, M. C., Bibby, T. S., & Poulton, A. J. (2010). Summertime trends in pelagic biogeochemistry at the porcupine abyssal plain study site in the northeast Atlantic. *Deep-Sea Research Part II*, *57*(15), 1313–1323. https://doi.org/10.1016/j.dsr2.2010.01.008

Painter, S. C., Sanders, R., Poulton, A. J., Woodward, E. M. S., Lucas, M., & Chamberlain, K. (2007). Nitrate uptake at photic zone depths is not important for export in the subtropical ocean. *Global Biogeochemical Cycles*, *21*(4), GB4005. https://doi.org/10.1029/2006gb002807

Painter, S. C., Sanders, R., Waldron, H. N., Lucas, M. I., Woodward, E. M. S., & Chamberlain, K. (2008). Nitrate uptake along repeat meridional transects of the Atlantic Ocean. *Journal of Marine Systems*, *74*(1–2), 227–240. https://doi.org/10.1016/j.jmarsys.2007.12.009

Poulton, A. J., Sanders, R., Holligan, P. M., Stinchcombe, M. C., Adey, T. R., Brown, L., & Chamberlain, K. (2006). Phytoplankton mineralization in the tropical and subtropical Atlantic Ocean. *Global Biogeochemical Cycles*, *20*(4), GB4002. https://doi.org/10.1029/2006gb002712

Ragueneau, O., Savoye, N., Del Amo, Y., Cotton, J., Tardiveau, B., & Leynaert, A. (2005). A new method for the measurement of biogenic silica in suspended matter of coastal waters: UsingSi: Al ratios to correct for the mineral interference. *Continental Shelf Research*, *25*(5–6), 697–710. https://doi.org/10.1016/j.csr.2004.09.017

Ragueneau, O., & Treguer, P. (1994). Determination of biogenic silica in coastal waters: Applicability and limits of the alkaline digestion method. *Marine Chemistry*, *45*(1–2), 43–51. https://doi.org/10.1016/0304-4203(94)90090-6

R Core Team. (2024). *R: A language and environment for statistical computing*. R Foundation for Statistical Computing. Retrieved from https://www.R-project.org/

Redfield, A. C., Ketchum, B. H., & Richards, F. A. (1963). The influence of organisms on the composition of sea-water. In M. N. Hill (Ed.), *The sea: Vol 2: Composition of seawater comparative and descriptive oceanography* (pp. 26–77). Interscience.

Rees, A. P., Joint, I., & Donald, K. M. (1999). Early spring bloom phytoplankton-nutrient dynamics at the Celtic sea shelf edge. *Deep-Sea Research Part I*, *46*(3), 483–510. https://doi.org/10.1016/s0967-0637(98)00073-9

Rees, A. P., Woodward, E. M. S., & Joint, I. (2006). Concentrations and uptake of nitrate and ammonium in the Atlantic Ocean between 60°N and 50°S. *Deep-Sea Research Part II*, *53*(14–16), 1649–1665. https://doi.org/10.1016/j.dsr2.2006.05.008

Sanders, R., Henson, S. A., Koski, M., De La Rocha, C. L., Painter, S. C., Poulton, A. J., et al. (2014). The biological carbon pump in the North Atlantic. *Progress in Oceanography*, *129*, 200–218. https://doi.org/10.1016/j.pocean.2014.05.005

Sieracki, M. E., Verity, P. G., & Stoecker, D. K. (1993). Plankton community response to sequential silicate and nitrate depletion during the 1989 North Atlantic spring bloom. *Deep-Sea Research Part II*, *40*(1–2), 213–225. https://doi.org/10.1016/0967-0645(93)90014-e

Slawyk, G., Collos, Y., & Auclair, J. (1977). The use of the ^{13}C and ^{15}N isotopes for the simultaneous measurement of carbon and nitrogen turnover rates in marine phytoplankton. *Limnology & Oceanography*, *22*(5), 925–932. https://doi.org/10.4319/lo.1977.22.5.0925

Sommer, U., & Lengfellner, K. (2008). Climate change and the timing, magnitude, and composition of the phytoplankton spring bloom. *Global Change Biology*, *14*(6), 1199–1208. https://doi.org/10.1111/j.1365-2486.2008.01571.x

Sundby, S., Drinkwater, K. F., & Kjesbu, O. S. (2016). The North Atlantic spring-bloom system—Where the changing climate meets the winter dark. *Frontiers in Marine Science*, *3*, 28. https://doi.org/10.3389/fmars.2016.00028

Terhaar, J., Burger, F. A., Vogt, L., Frolicher, T. L., & Stocker, T. F. (2025). Record sea surface temperature jump in 2023–2024 unlikely but not unexpected. *Nature*, *639*(8056), 942–946. https://doi.org/10.1038/s41586-025-08674-z

Tilstone, G., Smyth, T., Poulton, A., & Huston, R. (2009). Measured and remotely sensed estimates of primary production in the Atlantic Ocean from 1998 to 2005. *Deep-Sea Research Part II*, *56*(15), 918–930. https://doi.org/10.1016/j.dsr2.2008.10.034

Tilstone, G. H., Land, P. E., Pardo, S., Kerimoglu, O., & Van der Zande, D. (2023). Threshold indicators of primary production in the North-East Atlantic for assessing environmental disturbances using 21 years of Satellite Ocean colour. *Science of the Total Environment*, *854*, 158757. https://doi.org/10.1016/j.scitotenv.2022.158757

Varela, M. M., Bode, A., Fernandez, E., Gonzalez, N., Kitidis, V., Varela, M., & Woodward, E. M. S. (2005). Nitrogen uptake and dissolved organic nitrogen release in planktonic communities characterised by phytoplankton size-structure in the central Atlantic Ocean. *Deep-Sea Research Part I*, *52*(9), 1637–1661. https://doi.org/10.1016/j.dsr.2005.03.005

Wood, E. S. (1992). *The community photosynthetic quotient and the assimilation of nitrogen by oceanic plankton. School of ocean sciences*. PhD thesis. University College of North Wales (Bangor). (p. 503).

References From the Supporting Information

Adcroft, A., & Campin, J.-M. (2004). Rescaled height coordinates for accurate representation of free-surface flows in ocean circulation models. *Ocean Modelling*, *7*(3–4), 269–284. https://doi.org/10.1016/j.ocemod.2003.09.003

Aldama-Campino, A., Döös, K., Kjellsson, J., & Jönsson, B. (2020). TRACMASS: Formal release of version 7.0 (version v7.0-beta). *Zenodo*. https://doi.org/10.5281/zenodo.4337926

Amino, T., Iizuka, Y., Matoba, S., Shimada, R., Oshima, N., Suzuki, T., et al. (2021). Increasing dust emission from ice free terrain in southeastern Greenland since 2000. *Polar Science*, *27*, 100599. https://doi.org/10.1016/j.polar.2020.100599

Batrak, Y., & Müller, M. (2019). On the warm bias in atmospheric reanalyses induced by the missing snow over Arctic sea-ice. *Nature Communications*, *10*(1), 4170. https://doi.org/10.1038/s41467-019-11975-3

Bullard, J. E., & Mockford, T. (2018). Seasonal and decadal variability of dust observations in the Kangerlussuaq area, west Greenland. *Arctic Antarctic and Alpine Research*, *50*(1), S100011. https://doi.org/10.1080/15230430.2017.1415854

Bullard, J. E., Baddock, M., Bradwell, T., Crusius, J., Darlington, E., Gaiero, D., et al. (2016). High-latitude dust in the Earth system. *Reviews of Geophysics*, *54*(2), 447–485. https://doi.org/10.1002/2016rg000518

Döös, K., Jönsson, B., & Kjellsson, J. (2017). Evaluation of oceanic and atmospheric trajectory schemes in the TRACMASS trajectory model v6.0. *Geoscientific Model Development*, *10*(4), 1733–1749. https://doi.org/10.5194/gmd-10-1733-2017

Embury, O., Merchant, C. J., Good, S. A., Rayner, N. A., Hyer, J. L., Atkinson, C., et al. (2024). Satellite based time-series of sea-surface temperature since 1980 for climate applications. *Scientific Data*, *11*(1), 326. https://doi.org/10.1038/s41597-024-03147-w

Guiavarc'h, C., Storkey, D., Blaker, A. T., Blockley, E., Megann, A., Hewitt, H., et al. (2025). GOSI9: UK global ocean and sea ice configurations. *Geoscientific Model Development*, *18*(2), 377–403. https://doi.org/10.5194/gmd-18-377-2025

Hersbach, H., Bell, B., Berrisford, P., Hirahara, S., Horányi, A., Muñoz-Sabater, J., et al. (2020). The ERA5 global reanalysis. *Quarterly Journal of the Royal Meteorological Society*, *146*(730), 1999–2049. https://doi.org/10.1002/qj.3803

Locarnini, R. A., Mishonov, A. V., Baranova, O. K., Reagan, J. R., Boyer, T. P., Seidov, D., et al. (2024). *World ocean atlas 2023, volume 1: Temperature. A* (Vol. 89). Mishonov Technical Ed. NOAA Atlas NESDIS. https://doi.org/10.25923/54bh-1613

Meinander, O., Dagsson-Waldhauserova, P., Amosov, P., Aseyeva, E., Atkins, C., Baklanov, A., et al. (2022). Newly identified climatically and environmentally significant high-latitude dust sources. *Atmospheric Chemistry and Physics*, *22*(17), 11889–11930. https://doi.org/10.5194/acp-22-11889-2022

Madec, G., & the NEMO System Team. (2024). *NEMO ocean engine reference manual*. Zenodo. https://doi.org/10.5281/zenodo.1464816

Merchant, C. J., Embury, O., Bulgin, C. E., Block, T., Corlett, G. K., Fiedler, E., et al. (2019). Satellite-based time-series of sea-surface temperature since 1981 for climate applications. *Scientific Data*, *6*(1), 223. https://doi.org/10.1038/s41597-019-0236-x

Reagan, J. R., Seidov, D., Wang, Z., Dukhovskoy, D., Boyer, T. P., Locarnini, R. A., et al. (2024). *World ocean atlas 2023, volume 2: Salinity. A. Mishonov* (Technical Editor). NOAA Atlas NESDIS 90. https://doi.org/10.25923/70qt-9574

Storkey, D., Blaker, A. T., Mathiot, P., Megann, A., Aksenov, Y., Blockley, E. W., et al. (2018). UK global ocean GO6 and GO7: A traceable hierarchy of model resolutions. *Geoscientific Model Development*, *11*(8), 3187–3213. https://doi.org/10.5194/gmd-11-3187-2018

Tjernström, M., & Graversen, R. G. (2009). The vertical structure of the lower Arctic troposphere analysed from observations and the ERA-40 reanalysis. *Quarterly Journal of the Royal Meteorological Society*, *135*, 431–443. https://doi.org/10.1002/qj.380

Tsujino, H., Urakawa, S., Nakano, H., Small, R. J., Kim, W. M., Yeager, S. G., et al. (2018). JRA-55 based surface dataset for driving ocean–sea-ice models (JRA55-do). *Journal of Hydrometeorology*, *130*, 79–139. https://doi.org/10.1016/j.ocemod.2018.07.002

Vancoppenolle, M., Rousset, C., Blockley, E., Aksenov, Y., Feltham, D., Fichefet, T., et al. (2023). SI3, the NEMO sea ice engine (4.2release_doc1.0). *Zenodo*. https://doi.org/10.5281/zenodo.7534900

Zampieri, L., Arduini, G., Holland, M., Keeley, S. P. E., Mogensen, K., Shupe, M. D., & Tietsche, S. (2023). A machine learning correction model of the winter clear-sky temperature bias over the Arctic sea ice in atmospheric reanalyses. *Monthly Weather Review*, *151*(6), 1443–1458. https://doi.org/10.1175/MWR-D-22-0130.1